

## Anti-CSF-1R therapy with combined immuno- chemotherapy coordinate an adaptive immune response to eliminate macrophage enriched Triple Negative Breast Cancers.

Diego A. Pedroza<sup>1,2,3</sup>, Xueying Yuan<sup>1,3,5</sup>, Fengshuo Liu<sup>1,2,3,5</sup>, Hilda L. Chan<sup>1,2,3,6</sup>, Christina Zhang<sup>1</sup>, William Bowie<sup>2,3,5</sup>, Alex J. Smith<sup>1,3,5</sup>, Sebastian J. Calderon<sup>1</sup>, Nadia Lieu<sup>1</sup>, Weiguo Wu<sup>7</sup>, Paul Porter<sup>7</sup>, Poonam Sarkar<sup>8</sup>, Na Zhao<sup>1,3</sup>, Constanze V. Oehler<sup>1</sup>, Ondrej Peller<sup>1</sup>, M. Waleed Gaber<sup>8</sup>, Qian Zhu<sup>2,3,4</sup>, Charles M. Perou<sup>9</sup>, Xiang H-F. Zhang<sup>1,2,3,10</sup> and Jeffrey M. Rosen<sup>1,3\*</sup>

<sup>1</sup>Department of Molecular and Cellular Biology, Baylor College of Medicine, One Baylor Plaza, Houston, TX, 77030, USA.

<sup>2</sup>Lester and Sue Smith Breast Center, Baylor College of Medicine, One Baylor Plaza, Houston, TX 77030, USA.

<sup>3</sup>Dan L. Duncan Comprehensive Cancer Center, Baylor College of Medicine, One Baylor Plaza, Houston, TX, 77030, USA.

<sup>4</sup>Department of Molecular and Human Genetics, Baylor College of Medicine, One Baylor Plaza, Houston, TX, 77030, USA.

<sup>5</sup>Graduate Program in Cancer and Cell Biology, Baylor College of Medicine, One Baylor Plaza, Houston, TX 77030, USA.

<sup>6</sup>Medical Scientist Training Program, Baylor College of Medicine, Houston, TX 77030, USA

<sup>7</sup>Cytometry and Cell Sorting Core, Baylor College of Medicine, One Baylor Plaza, Houston, TX 77030, USA.

<sup>8</sup>Department of Pediatrics, Baylor College of Medicine, One Baylor Plaza, Houston, TX 77030, USA.

<sup>9</sup>Lineberger Comprehensive Cancer Center, University of North Carolina, 450 West Dr, Chapel Hill, NC, 27599, USA.

<sup>10</sup>McNair Medical Institute, Baylor College of Medicine, One Baylor Plaza, Houston, TX 77030, USA.

\*Correspondence: [jrosen@bcm.edu](mailto:jrosen@bcm.edu).

## ABSTRACT

Patients diagnosed with metastatic triple negative breast cancer (mTNBC) have limited treatment options, are more prone to develop resistance and are associated with high mortality. A cold tumor immune microenvironment (TIME) characterized by low T cells and high tumor associated macrophages (TAMs) in mTNBC is associated with the failure of standard-of-care chemotherapy and immune checkpoint blockade (ICB) treatment. We demonstrate that the combination of immunomodulatory metronomic Cyclophosphamide (CTX) coupled with anti-CSF-1R antibody targeted therapy (SNDX-ms6352) and anti-PD-1 (ICB), was highly effective against aggressive metastatic syngeneic *Trp53* null TNBC genetically engineered mouse models (GEMMs) that present with high macrophage infiltration. Mechanistically, CSF-1R inhibition along with CTX disrupted the M-CSF/CSF-1R axis which upregulated IL-17, IL-15 and type II interferon resulting in elevated B- and T cell infiltration. Addition of an anti-PD-1 maintenance dose helped overcome de novo PD-L1 intra-tumoral heterogeneity (ITH) associated recurrence in lung and liver mTNBC.

## INTRODUCTION

Triple negative breast cancer (TNBC) is the most aggressive breast cancer with an overall poorer prognosis compared to other breast cancer subtypes (1). Newly approved immune checkpoint blockade (ICB) accompanied by cytotoxic chemotherapies can now be administered to TNBC patients (2). While multiple clinical trials have reported positive outcomes for TNBC including those utilizing these T cell activating agents (3),(4) the response rates in these patients vary and clearly more refined therapies are needed to improve patient survival especially in the metastatic setting. The Tumor Immune Microenvironment (TIME) in TNBC has been suggested to play a critical role in patient response. Tumor plasticity and the Epithelial-to-Mesenchymal Transition (EMT) (5) are critical for metastasis and a relationship exists between EMT and myeloid cells, particularly Tumor Associated Macrophages (TAMs) (6). Results from the ARTEMIS (NCT02276443) clinical trial show that TNBC patients with a high EMT/macrophage score failed to undergo a pathological Complete Response (pCR) following neoadjuvant chemotherapy (NACT) (7),(8). Furthermore, the clinical benefit of Immune Checkpoint Blockade (ICB) is modest and poor patient outcomes may be due in part to the presence of immunosuppressive macrophages within the TIME.

Most patients die from metastatic disease and as such metastatic breast cancer remains fatal for 97-99% of those diagnosed with a median survival of only 18-24 months (9). In the recently published AURORA trials, profiling of paired TNBC patient samples from the primary and metastatic site have shown an immunologically quiescent TIME in sites of metastasis as compared to the primary site, with the liver having the coldest TIME. Pathway analysis done on these samples have shown a downregulation of T- and B cell receptor signaling in the metastatic sites accompanied by an abundance of macrophages and neutrophils (10),(11). Several strategies have been deployed to therapeutically manipulate TAMs within TNBCs. These include macrophage reprogramming, using Class II HDAC inhibition (12) and the LPS derivate, monophosphoryl lipid A+INF $\gamma$  (13), phagocytic reactivation by CD47/SIRPalpha blockade with an anti-CD47 antibody (14), and recruitment inhibition or depletion by both small molecule and antibody based targeting of either the CSF-1/CSF-1R axis (15), (16), (17) or the CCL2/CCR2 axis (18).

Previously, we reported that the combination of CTX coupled with pharmacologic inhibition of TAMs by Pexidartinib (PLX-3397), a CSF-1R small molecule inhibitor, was highly effective against aggressive, claudin-low murine mammary tumors in several syngeneic *Trp53* null TNBC genetically engineered mouse models (GEMMs) that present with high TAM infiltration. Using scRNA-seq we found that T helper cells coordinated with antigen presenting B cells to promote anti-tumor immunity and long-term responses. Using high dimensional imaging techniques, we further identified the close spatial localization of B220<sup>+</sup> CD86<sup>+</sup> activated B cells with CD40lg<sup>+</sup> CD4<sup>+</sup> T cells within tertiary lymphoid structures (TLSs) that were present up to six weeks post treatment in primary tumors. However, recent studies from the I-SPY 2 (NCT01042379) clinical trial demonstrated that although, the small molecule inhibitor PLX-3397 successfully depleted macrophages, off target effects on other tyrosine kinases along with liver toxicity prevented it from moving forward for the treatment of TNBC (19).

TAMs have been demonstrated to be transcriptionally distinct from their monocytic and tissue-resident macrophage counterparts (20). Interestingly a 37-gene TAM signature associated with high CSF1 has been observed in aggressive ER/PR negative breast cancers (20),(21). Thus, inhibiting the CSF-1/CSF-1R axis remains an attractive mechanism within the TIME for the treatment of aggressive TNBCs. To overcome toxicity and off target limitations, we utilized SNDX-ms6352 (Axatilimab-csfr), a mAb with high affinity for CSF-1R, which was recently FDA approved for the treatment of chronic graft-versus-host disease (cGVHD) AGAVE-201 (NCT04710576) (22). Using several *Trp53* null TNBC models we demonstrate that SNDX-ms6352 combined with CTX increased the levels of M-CSF along with type II interferon in primary tumors. However, ITH within the metastatic TIME of lung metastases led to recurrence with some residual tumor cells expressing increased expression of PD-L1. Thus, a maintenance dose of ICB was employed to reinvigorate the metastatic TIME of lung and liver metastases in order to prolong the overall survival and achieve a complete response (CR). Functionally, treatment cessation, tumor cell rechallenges, adaptive T cell transfer, possible TLS formation along with infiltration of tumor infiltrating lymphocytes (TILs) confirmed long-term anti-tumor adaptive immunity. These findings have provided the foundation for the novel combination (New) of low dose oral cyclophosphamide (S) To potentiate

Axatilimab-csfr (A) + retifanlimab (R) in treating mTNBC (NEW START) as a phase Ib clinical trial.

## RESULTS

### **CSF-1R inhibition coupled with CTX leads to a type II interferon response in primary macrophage enriched TNBC pre-clinical GEMMS.**

To study the effects of therapeutically targeting the CSF-1/CSF-1R axis we treated several *Trp53* null TNBC GEMMs using SNDX-ms6352, a novel high affinity anti-CSF-1R mAb coupled with low-dose metronomic Cyclophosphamide (CTX). These *Trp53* null syngeneic GEMMs mimic a spectrum of human breast cancer subtypes, including luminal, basal-like and claudin-low making them heterogenous (23),(6). Loss of *TP53* is observed in patients with advanced metastatic disease and is considered a biomarker of poor prognosis (24),(25). Not surprisingly up to 91% of patients diagnosed with TNBC can carry a *TP53* mutation (26).

Spatial profiling via imaging mass cytometry (IMC) revealed highly proliferative Vimentin<sup>+</sup> tumor cells within the claudin-low T12, 2151R, T11 models, and pan-CK<sup>+</sup> tumor cells in the basal- 2336R GEMM. The claudin-low and basal-like models exhibit low CD8<sup>+</sup> T cell infiltration and high F4/80<sup>+</sup> TAMs, while the 2208L luminal-like tumors had high S100A8/9<sup>+</sup> neutrophils (**Figures 1A, 1B and S1A-S1C**). Importantly, the claudin-low models display a mesenchymal architecture highly infiltrated by F4/80<sup>+</sup> macrophages and express high levels of the EMT marker vimentin similarly to what is observed in the patients with elevated EMT/macrophage levels.

Although, SNDX-ms6352 alone efficiently depleted F4/80<sup>+</sup> TAMs in T12 tumors via cleaved caspase-3 activation it had little to no impact on primary tumor growth (**Figures S1D-S1G**). Mechanistically, dose-dependent accumulation of CSF-1R was observed in T12 and 2151R TAMs *in vitro* (**Figure S1H and S1I**), likely due to ligand-receptor binding inhibition, prohibiting internalization and downstream activation that leads to cell death. To test the long-term efficacy of SNDX-ms6352 combined with CTX we designed a dose specific treatment schedule which included treatment cessation at day 28 (**Figure 1C**).

TAM inhibition by SNDX-ms6352 enhanced the immunostimulatory effects of CTX resulting in increased survival of all three claudin-low (T12, 2151R and T11) and the basal-like (2336R) GEMM (**Figure 1D**). We observed significant complete tumor regression in the two claudin-low (T12 and 2151R) TAM enriched models (**Figure 1D**). Interestingly, only the highly neutrophil enriched luminal-like 2208L model failed to respond to this combination treatment (**Figure 1D**). Intriguingly, both T12 and 2151R models were resistant to contralateral mammary tumor cell re-challenge (**Figure 1E, 1F and S1J**). Removal of the original and contralateral re-challenged mammary glands revealed increased infiltration of CD20<sup>+</sup> B cells in proximity to CD8<sup>+</sup> T cells (**Figure S1K**).

Next, to capture and profile the changes within the TIME we performed whole transcriptomic single cell RNA sequencing (scRNA-seq). For unbiased analysis we utilized a barcoding technology for cell multiplexing (CellPlex), which allowed us to sequence together the two models that yielded a CR (T12 and 2151R) (**Figure 1G**). Cumulatively the combination substantially showed differences in the abundance of T- and B cells and a decrease in macrophages (**Figure 1G**). Further, we observed elevated *Mrc1* and *Vim* following CTX administration, while SNDX-ms6352 depleted, *Csf1r*, *Mrc1*, *Trem2* and *Mki67* macrophage specific transcripts (**Figure S2A**). Although the combination treatment did not ablate all macrophages, only in the T12 model in this subset of macrophages was increased expression of the lipid chaperone protein *Fabp5* observed (**Figure S2B and S2D**). Transcriptionally, T12 has more abundant macrophage subtypes including Prolif-TAM and lipid associated (LA)-TAMs compared to 2151R (**Figure S2C and Supplementary tables S1-S9**). Gene ontology (GO) analysis of the combination treated residual inflammatory TAMs revealed increased pathway regulation and activation of T cells with interferon type II response, while lipid-associated TAMs show cytokine-mediated signaling, lymphocyte proliferation and collagen processing (**Figure 1H and 1I and Supplementary table S10 and S11**). Only TAM depletion with either SNDX-ms6352 or the combination treatment disrupted the CSF signaling network cell-cell communication between macrophages, monocytes, neutrophils and tumor cells (**Figure 1J**).

Cytokine profiling analysis of plasma from mice bearing T12 tumors post combination treatment revealed an increase in the levels of the pro T and NK cell stimulant IL-5 (27),(28),(29) type II interferon response, INF- $\gamma$  (30),(31), pro-inflammatory macrophage marker MIG (CXCL9) (32),(33) and anti-tumor response IL-4 (34) (**Figure 1K, S2E** and **Supplementary table S12**). Importantly both SNDX-ms6352 and the combination treatment increased M-CSF which appears to be a functional biomarker (**Figure 1K**). CTX alone increased the levels of IL-17, a pro-inflammatory cytokine that has dichotomous anti- and pro-tumor effects (35),(36). Interestingly, we observed elevated levels of G-CSF following SNDX-ms6352, confirming the ying and yang between macrophages and neutrophils observed previously (37),(6),(38),(15). Within the tumor lysate CTX upregulated MIG but also increased RANTES (CCL5) a known macrophage recruiting cytokine (39), and this could potentially explain why tumors recur post CTX treatment cessation (**Figure S2F** and **Supplementary table S13**). Further, tumor lysate cytokines from the combination treatment yielded elevated levels of IL-5 and G-CSF (**Figure S2F**). Intriguingly, no beneficial tumor regression was observed when T12 tumors were grown in T cell deficient nude mice and subjected to the same treatments (**Figure S2G**). Thus, we speculate that in primary tumors, the combination treatment leads to long-term anti-tumor immunity via activation of pro-inflammatory pathways including type II interferon coupled with T, B and NK cell recruitment (**Figure S2H**).

### **Elevated PD-1/PD-L1 axis is associated with ITH associated recurrence in lung metastases.**

TNBC is an aggressive highly invasive subtype with high degree of visceral metastasis including metastasis to the lung (40) and liver (41). Both are associated with the worst prognosis and survival rates for breast cancer. Since macrophage depletion coupled with CTX disrupted the TIME which led to a sustained immunological response for primary tumors, we determined if the combination similarly altered the TIME in lung metastatic sites. To test the long-term efficacy of the combination we designed a similar treatment schedule as the primary tumors which included treatment cessation at day 28 (**Figure 2A**). Because luciferase and green fluorescent protein (GFP) are considered fluorophore-

immunogenic neoantigens (42),(43),(44),(45) we did not use them to track metastases. Thus, lung metastases were generated using 30,000 freshly dissociated (unlabeled) T12 tumor cells. Bromodeoxyuridine (BrdU) was utilized to identify (ID) established metastases post 12-day TV injection (**Figure 2B** and **S3A**). Although, a single dose of SNDX-ms6352 efficiently depleted F4/80<sup>+</sup> TAMs in lung metastasis (**Figure S3B** and **S3C**) only the combination led to better survival even after treatment cessation (**Figure 2C**). Mice that exhibit lung metastases deteriorate rapidly, and single agent treated mice lost considerable body weight compared to CTX, or combination treated mice (**Figure 2D**). To study the landscape of the lung metastatic TIME we compared IgG Control lungs (Controls 1&2), and combination treated lungs (Combos 1&2) via IMC (**Figure 2E**). Controls 1&2 expressed immunologically cold, highly proliferative macro-metastases (Ki67<sup>+</sup>, Vim<sup>+</sup>, CD44<sup>+</sup>) with infiltration of F4/80<sup>+</sup> TAMs and S100A8/9<sup>+</sup> neutrophils (**Figure S3D**). Although Combos 1&2 expressed decreased proliferative tumor cells (Ki67<sup>+</sup>, Vim<sup>+</sup>, CD44<sup>+</sup>) these immunologically cold micro-metastases displayed elevated levels of exhaustion markers PD-L1 and PD-1 (**Figure 2F-2H** and **S3E**). Intriguingly, IMC uncovered multiple micro-metastases adjacent to each other and each had its own unique phenotype, even though spatially they were in close proximity (**Figure S3F** and **S3G**). Thus, we determined if the ITH observed within the metastatic TIME might account for the suppression of long-term immunity leading to recurrence. Our previous observations of B- and T cell accumulation within the mammary gland of primary tumor cell-rechallenged mice, led us to speculate that a similar pattern would occur in the metastatic setting. However, following tumor cell rechallenge, prior to any tumor growth in the mammary gland all the mice exhibited lung metastatic recurrence (**Figure 2I**). Moreover, H&E and IHC identified an immunologically cold TIME with high levels of F4/80<sup>+</sup> TAMs (**Figure S3H**). Activation of the immune checkpoint (PD-1/PDL-1) axis can lead to tumor cell chemoresistance and is associated with increased metastasis (46).

**Addition of ICB reshapes the landscape of the metastatic TIME that leads to a T cell and neutrophil proximity response and inhibition of the PD-1/PD-L1 axis.**

We hypothesized that ITH within the lung metastatic TIME which displayed PD-L1 led to a dual effect resulting in F4/80<sup>+</sup> TAM accumulation and T cell repression and exhaustion. This might account for the presence of an immunologically cold environment and eventual recurrence following tumor cell-rechallenge. PD-L1 is a well-known T cell exhaustion marker that is not commonly observed in non-metastatic breast cancer. However, it has been observed in up to 30-60% of patients with metastatic TNBC (47),(48),(49). Therapeutic intervention of this axis can re-activate exhausted T cells within the TIME and lead to anti-tumor immunity (50). To directly compare the metastatic TIME between differing combinations which included the triple combination of CTX with SNDX-ms6352 and anti-PD-1, all lungs were harvested at day 7 post treatment (**Figure 3A**). For short-term studies treatment administration was delayed until day 19 to ensure that all treated samples had a sufficient metastatic burden for analysis (**Figure 3A**). Single agent and double combination treated mice lost a significant body weight as compared to mice that received additional ICB (**Figure 3B**). Using a previously published size-based scoring system (51), both the double and triple combination treated mice had a significantly lower metastatic score compared to single agent treated mice (**Figure 3C, 3D and S4A, Supplementary table 14**). IMC analysis revealed changes to the metastatic TIME. Both double and triple combinations decreased proliferative tumor cells (Ki67<sup>+</sup>, Vimentin<sup>+</sup> and CD44<sup>+</sup>) and TAMs (F4/80<sup>+</sup>) compared to single agent treatments (**Figure 3E and S4B-S4D**). Interestingly, we observed CD4<sup>+</sup>, CD8<sup>+</sup> T cells and S100A8/9<sup>+</sup> neutrophils within the tumor following combination treatments (**Figure 3E, 3F and S4E**). Independent single cell unsupervised cluster analysis identified several individual clusters in IgG controls that included Ki67/ vimentin while the triple combination consistently expressed CD11b/ Ly6C/ B220 and Ly6c/ CD4/ CD8 (**Figure S4E and S4F, S4G**). Importantly, only the double combination treatment showed an increase in PD-L1/PD-1 compared to the triple combination, consistent with our previous observations (**Figure 3G**). The addition of ICB depleted the PD-L1/PD-1 axis in inhibitory TAMs and increased the number and proximity of T cells and neutrophils to the tumor bed driving an anti-tumor response (**Figure 3H**).

## Triple combination leads to a long-term anti-tumor response of established lung metastases.

To assess the long-term efficacy of SNDX-ms6352 and CTX with ICB on established lung metastases, we repeated these initial experiments and injected 30,000 freshly dissociated (unlabeled) T12 tumor cells into the TV. To mimic what recently has been introduced in the clinic, we included a separate group that received a maintenance dose of ICB post 28-day treatment cessation (52). In this experiment the mice were monitored for up to 70 days to assess recurrence (**Figure 4A**). Single agent therapies, IgG control and anti-PD-1 had modest effects compared to the double and triple combination (**Figure 4B**). However, only the mice that continued to receive a maintenance dose of anti-PD-1 post treatment cessation had better survival (**Figure 4B**). The mice that received the triple combination tolerated the maintenance dose and preserved body weight, even when treated for up to 70 days (**Figure 4C**). To test systemic innate immunity, the mice were rechallenged at the mammary gland. Intriguingly the rechallenged mice impeded primary tumor growth compared to naïve control mice (**Figure 4D**). IF staining confirmed a decrease of BrdU<sup>+</sup> tumor cells, loss of CSF-1R signal and infiltration of CD20<sup>+</sup> B and CD8<sup>+</sup> T cells following the double combination in lung metastases (**Figure 4F** and **S5A**). We identified the close spatial localization of CD20<sup>+</sup> B cells with CD8<sup>+</sup> T cells within putative TLSs, which were only observed following the triple combination (**Figure 4E** and **4F**). Further, IHC confirmed loss of F4/80<sup>+</sup> TAMs and accumulation of S100A8<sup>+</sup> neutrophils and CD4<sup>+</sup>, CD8<sup>+</sup> T cells within lung metastases following the triple combination (**Figure S5B** and **S5C**).

## Immunologically cold T12 liver metastases are highly infiltrated by TAMs

Patients diagnosed with TNBC liver metastases are associated with significant morbidity and have the worst overall survival compared to other breast cancer subtypes with liver metastases (53),(54). These patients also exhibit lower immunotherapy efficacy via macrophage T cell killing mechanisms (55). We speculated that the new combination designed to eliminate TAMs with SNDX-ms6352 coupled to CTX and ICB that potentiates T cells in lung metastases might also be efficacious in the treatment of liver metastases.

Thus, we proceeded to generate organ specific liver metastases by injecting 5,000 freshly dissociated (unlabeled) T12 tumor cells into the portal vein (PV) (56) (**Figure 5A**). Intriguingly, the liver metastases were highly infiltrated by F4/80<sup>+</sup> TAMs and S100A8<sup>+</sup> neutrophils and devoid of CD8<sup>+</sup> T cells, while CD4<sup>+</sup> T cells remained spatially distant from the metastases (**Figure 5B**). H&E and BrdU staining were utilized to identify established metastases post 15-day PV injection (**Figure 5C**). To study the metastatic TIME of liver metastases all liver tissues were harvested at day 5-7 post IgG Control, SNDX-ms6352, CTX and CTX+SNDX-ms6352+/-anti-PD-1 (**Figure 5D**). Only the triple combination treated mice, maintained body weight (**Figure 5E**) and both the double and triple combination treated mice exhibited a lower metastatic score compared to single agent treated mice (**Figure 5F, 5G and S6A, Supplementary table 15**). Compared to IgG control, SNDX-ms6352 decreased F4/80<sup>+</sup> TAMs and S100A8/9<sup>+</sup> neutrophils. CTX induced CD4/CD8<sup>+</sup> T cells and also upregulated Pan-CK, F4/80<sup>+</sup> TAMs and PD-L1 (**Figure 5H, 5I and S6B**). In contrast, the double combination increased PD-1 the triple combination displayed modest elevated levels of CD4, Pan-CK and PD-L1 (**Figure 5H-5J and S6B**). However, unlike single agents including CTX both double and triple combinations decreased Ki67<sup>+</sup>, Vimentin<sup>+</sup> proliferative tumor cells and F4/80<sup>+</sup> TAMs. Single cell unsupervised cluster analysis identified several individual clusters similar to the lung metastatic TIME. IgG controls displayed elevated Ki67/Vimentin/CD44 and CD44/F4/80 while the triple combination had clusters that consistently displayed S100A8/9 with B220 B cells and CD4/CD8a T cells (**Figure S6C and S6D**). Loss of F4/80 TAMs was accompanied by close spatial localization of CD4/CD8<sup>+</sup> T cells to tumor cells following the triple combination (**Figure S6E**). In addition, Ly6G<sup>+</sup> S100A8/9<sup>+</sup> neutrophils surrounded the tumor cells (**Figure S6E and S6F**). Furthermore, SNDX-ms6352 efficiently depleted F4/80<sup>+</sup> TAMs within the liver metastatic tumor bed without affecting F4/80<sup>+</sup> Kupffer cells in the surrounding liver stroma (**Figure S6G**).

**Addition of ICB maintenance dose is necessary to generate adaptative anti-tumor immunity and eradicate established liver metastases.**

To assess the long-term efficacy of the triple combination along with a maintenance dose of anti-PD-1 on established liver metastases, we repeated our experiments and injected 5,000 freshly dissociated (unlabeled) T12 tumor cells into the PV. Similarly to our previous experiment we assessed recurrence for up to 56 days post 28-day treatment cessation (**Figure 6A**). For liver metastases we used PET/CT to detect fluorine-18 labeled fluorooxyglucose (<sup>18</sup>F-FDG) which identified and confirmed established liver metastases post 15-day PV injections (day 0) (**Figure 6B**). The same mice were imaged at day 56 (post-treatment) and had visibly and quantitatively less liver metastases following CTX+SNDX-ms6352+aPD-1 (m.dose) (**Figure 6C**). CTX and double combination-treated mice, significantly increased overall survival compared to IgG control and SNDX-ms6352-treated mice, however, only mice that received the triple combination had better survival (**Figure 6D**). Remarkably 66% of the mice that received an ICB maintenance dose post treatment cessation achieved a CR (**Figure 6D**). CTX, double and triple combination treated mice preserved body weight for up to 56 days (**Figure 6E**). IF staining demonstrated decreased levels of CSF-1R following SNDX-ms6352 compared to IgG control. However, in liver metastases only the triple combination displayed increased CD20<sup>+</sup> B and CD8<sup>+</sup> T cells (**Figure 6F, 6G and S7A**). IHC confirmed diminished levels of F4/80<sup>+</sup> TAMs following SNDX-ms6352, and in the double and triple combination-treated mice. Importantly only the triple combination displayed high CD8<sup>+</sup> and CD4<sup>+</sup> T cells and S100A8<sup>+</sup> neutrophils consistent with our previous observations (**Figure S7B and S7C**). Impressively 100% of the mice cleared the mammary gland tumor cell rechallenge (**Figure 6H and S7D**). To further test the adaptive immunity of these mice we isolated splenocytes (CD3<sup>+</sup> T cells) and performed an adoptive T cell transfer (ACT) into T12 tumor bearing mice (**Figure 6I**). Because of the possibility of immediate T cell exhaustion, we tested if a single dose of anti-PD-1 would benefit the ACT. Intriguingly the addition of anti-PD-1 with T cells significantly slowed the growth of tumor bearing mice compared anti-PD-1 and T cells alone (**Figure 6J and S7E**). These mice also had significantly smaller spleens compared to mice that received IgG control, anti-PD-1 and T cells alone (**Figure 6K**) and this correlated with a positive outcome (57),(58). The spleens and tumors of the mice that received anti-PD-1 treatment along with T cells contained higher levels of CD8<sup>+</sup>

T cells (**Figure 6L, 6M and S7F, S7G**). The rechallenged mice displayed systemic anti-tumor immunity and ACT donor mice most likely benefited from central memory T cells.

**TNBC patients display elevated immunosuppressive macrophage signatures in metastatic sites compared to primary tumors.**

In the metastatic setting our data suggest that our models resemble an immunologically cold TIME with an abundance of TAMs that are specifically devoid of T cells. Thus, we analyzed the transcriptomic dataset of TNBC patients from the AURORA clinical study (**GSE209998**) which genetically profiled matched metastatic and primary breast cancers (**Figure 7A**) (11). We determined if any clinical correlations existed between the metastatic TIME of patients and that of T12 lung and liver metastases using multiple immune subsets and specific macrophage signatures. CIBERSORTx signatures revealed an overactive TIME that upregulated multiple T cell (CD3, CD8 and CD4), natural killer (NK) cell, memory B and CD19 B cell, as well as several monocyte and macrophage immunity (M0 and M1) signatures compared to matched lung or liver metastases (**Figure 7B**). This correlated in patients with varying breast cancer subtype (LumA, LumB and HER2E) (**Figure S7A**). However, lung and liver metastatic sites exhibited increased claudin-low associated gene signatures with several patients having signatures that phenocopy the p53 null mouse models (MM) (**Figure 7B**). Individual gene expression profiling identified significantly increased immunosuppressive macrophage signatures, *CSF1R* (59), *MRC1* (60) and *TREM2* (61) in metastases compared to primary tumors (**Figure 7C**). Unbiased gene expression profiling between metastatic sites vs primary tumors showed upregulation of the known TAM marker *CD163* (62),(63) and *CXCL11* a macrophage-derived chemokine (64),(65),(66). More in-depth analysis between organ specific metastases revealed upregulation of the transcription factor hes family BHLH transcription factor 2 (*HES2*) in lung vs breast, the p53 degrader ubiquitin D (*UBD*) in liver vs breast and the preferentially expressed antigen of melanoma (*PRAME*) gene in liver vs lung, which has been observed in metastatic breast cancers (**Figure S7B**) (67). Although, gene expression profiles will never be identical between murine models and humans, in this study we showed that similar immune profiles, specifically macrophage

associated genes do exist between the metastatic TIME of murine models and that of human metastatic samples. In summary, our study demonstrates that administration of ICB along with combination anti-CSF1R and low dose CTX therapy was able to reshape the metastatic landscape of lung and liver metastases resulting in increased TILs with B cells and neutrophils, prolonged survival and a CR (**Figure 8**).

## DISCUSSION

TAMs have been readily observed in multiple types of cancers including breast and are associated with poorer response to both chemo- and immunotherapies (68),(69),(70),(71),(72),(8). In breast cancers a correlation between TAMs and TILs exists, with the former being highly upregulated compared to the latter (73),(8). Preclinical efforts to target TAMs in TNBC have previously demonstrated positive outcomes. For instance, anti-CSF-1R antibody therapy successfully reduced F4/80<sup>+</sup> TAMs to overcome PARPi resistance in a BRCA1-deficient TNBC model mediated by CD8<sup>+</sup> T cells (74). These results coincide with our previous findings where we showed a B- and T cell response using a small molecule inhibitor of CSF-1R, PLX-3397 in primary p53 null GEMMs (15). However, liver toxicity resulted in PLX-3397 being discontinued in the clinic for the treatment of TNBCs (19).

To efficiently target TAMs and limit toxicities we tested the recent FDA approved CSF-1R antibody SNDX-ms6352 (22). While SNDX-ms6352 depleted F4/80<sup>+</sup> TAMs it did not halt tumor growth, similar to what was observed with PLX-3397. In this study we combined SNDX-ms6352 with a metronomic dose of CTX which has been shown to be immunomodulatory in both murine models and patients (75),(76),(77). Preliminary studies from our laboratory revealed that that CTX reshapes the myeloid compartment of the bone marrow, ablating neutrophils and increasing monocytes locally and systemically. Post CTX treatment cessation leads to increased TAMs within the tumor bed. Therefore, only the combination treatment yielded a CR in the T12, 2151R claudin-low and 2336R basal-like models. Although 2151R was sensitive to CTX, tumor cell-rechallenged mice failed to reject tumor growth and lacked B- and T cell infiltration due to the absence of the adaptive immunity required to eliminate the cell rechallenge that was only provided by the

combination treatment. Single-cell transcriptomics and cytokine profiling confirmed T- and B cell infiltration with loss of immunosuppressive *Csf1r* and *Trem2* TAMs via increased levels of IL-5, IFN- $\gamma$ , IL-4 and MIG. Interestingly residual inflammatory/lipid associated T12 TAMs expressing *Fabp5* involved in lymphocyte activation and cytokine mediated pathways were observed. *Fabp5* is known to antagonize immunosuppressive macrophage related markers *Fizz1*, *CD206* and *Arg1* and is important for the maintenance and survival of CD8 $^{+}$  T cells (78),(79),(80). Successful CSF-1R inhibition (81) was indicated by the elevated expression of the M-CSF biomarker in the plasma.

Although, the treatment outcomes for primary tumors yielded impressive results, most TNBC patients die from metastatic disease (9) with metastatic TNBC having a 5-year survival rate of 11% and a median survival of 11-13 months (82). Thus, we tested the efficacy of the double combination treatment on two of the most prevalent sites of metastasis for TNBC, the lung and liver (40), (41). Women who present to the clinic have established metastatic lesions, thus we waited about 2 weeks post TV or PV injections to mimic what is being observed in the clinic. Prior to treatment H&E and BrdU incorporation were employed to determine the metastatic burden and ensure the presence of established lung or liver metastases. The metastatic TIME of the lungs displayed high levels of Vimentin $^{+}$ , CD44 $^{+}$ , tumor cells and F4/80 $^{+}$  TAMs. Although, the double combination was well tolerated, and several mice reached CR after 56 days. ITH was observed within the metastatic TIME displaying de-novo levels of PD-L1 within double combination treated mice followed by rapid recurrence of lung metastases. Furthermore, following tumor cell rechallenge these mice failed to generate systemic adaptive anti-tumor immunity. Intra-patient ITH (multiple nodules within the same individual patient) are associated with lower response rates, treatment insensitivity and resistance (83),(84).

Addition of ICB to SNDX-ms6352 and CTX resulting in sustained loss of TAMs, tumor cells and decreased PD-L1/PD-1 expression accompanied by B- and T cell residual TLSs. Established liver metastases exhibited an immunologically “cold” TIME. Although, we did not observe TLSs in the liver, the triple combination did increase B- and T cells. Impressively, this novel triple combination eradicated established liver metastases. Furthermore, systemic adaptive anti-tumor immunity was observed when T cells reduced

tumor burden following ACT. Importantly SNDX-ms6352 targeted F4/80<sup>+</sup> TAMs within the metastatic tumor bed, but spared the majority of Kupffer cells within the liver. In clinical trials, the observed effects of Axatilimab-csfr which increased liver enzymes may be attributed to a decrease in Kupffer cells; however, these changes did not lead to organ damage (22). To evaluate the potential clinical significance of these findings, we analyzed results from the AURORA trial, one of the most up to date and unique breast cancer specific clinical studies that encompasses primary tumors with matched metastatic samples. Transcriptomic datasets of TNBC patients from the AURORA metastatic clinical study (**GSE209998**) which genetically profiled matched metastatic and primary breast cancers (11), show upregulated T cell natural killer cell, memory and B cell, monocyte and macrophage CIBERSORTx signatures in primary tumors as compared to matched lung or liver metastases. Importantly, patients with metastatic disease had increased immunosuppressive macrophage signatures compared to primary tumors and displayed a colder TIME specially in the liver. Within the limitations of these cross-species analyses, we observe similar immune profiles, specifically an immunologically cold TIME does exist between lung and liver metastases of murine models and that of human metastatic samples. Spatially resolved metastatic breast cancer maps, similarly, identified macrophages as the most abundant immune cells, specifically in patients that had not received ICB (85),(86).

Although both lung and liver metastases exhibited similarly low immune profiles, the liver was immunologically colder, which mirrors what has been observed in the AURORA clinical studies. Interestingly, in primary tumors T12 is devoid of S100A8/9<sup>+</sup> neutrophils. However, S100A8/9<sup>+</sup> neutrophils were now observed within the boundary of tumor metastases, and in liver metastases S100A8/9<sup>+</sup> neutrophils were observed within the tumor bed near F4/80<sup>+</sup> TAMs. Interestingly, we observed that Ly6G<sup>+</sup> S100A8/9<sup>+</sup> neutrophils post triple combination surrounded Vim<sup>+</sup> CD44<sup>+</sup> tumor cells within the liver. We speculate that although neutrophils can support pro-tumorigenic functions, they can also directly target tumor cells (87), therefore potentially converting them from tumor supporting to tumor-inhibitory TANs. Further studies are required to support this hypothesis.

Patients diagnosed with mTNBC will often continue to be treated for the remainder of their lives (88). The new standard of care (SOC) for mTNBC now often includes immunotherapy (89),(90) with the addition of anti-PD-1 (91),(92). Accordingly in the current study we demonstrated that a maintenance dose of ICB post treatment cessation of SNDX-ms6352 and CTX may be important to minimize the toxic side effects of CTX (52) and maximize treatment efficacy. Based upon these preclinical studies, this novel combination treatment study will now be tested in the clinic to treat patients with mTNBC, (NEW START clinical trial, SABCS abstract P2-12-26).

Due to the highly aggressive nature of the T12 claudin-low model, we have been unable to generate spontaneous metastatic models following resection. Thus, for this study we relied on experimental metastases via TV and PV injections. This approach generated organ specific metastases and allowed sufficient numbers of mice for control and treatment groups, but may not reflect all the properties of spontaneous metastasis. Moreover, several mice had to be ethically euthanized due to tumor growth within the tails. Reporters such as luciferase are known to be neoantigens that can affect treatment outcomes. Therefore, we abstained from using them to track metastases. Mice bearing lung metastases did not survive the PET/CT scans. While the results of this study were largely conducted on the T12 model, efforts to generate experimental metastases using basal-like models are underway.

Finally, although previous studies have used a variety of small molecule and antibodies targeting CSF-1R (NCT01494688, NCT02760797, NCT02435680, NCT02323191) and in some cases combined these with either anti-PD-1, anti-PD-L1 or other chemotherapy agents. The combination of immunostimulatory CTX with anti-CSF-1R and anti-PD-1 is unique and was required to promote long term durable immunity in lung and liver metastases. As shown single agents targeting CSF-1R or anti-PD-1 were ineffective. This highlights the importance of appropriate combinatorial therapies and the need to test them on established metastasis.

## METHODS

### Mouse Models

The mouse strains utilized, included female BALB/c mice obtained from Inotiv (strain 047) and female Hsd:Athymic Nude-*Foxn1<sup>nu</sup>*; from Inotiv (strain 069). The procedures used for in vivo animal models were conducted following protocol AN-504 approved by the Baylor College of Medicine Institutional Animal Care and Use Committee (IACUC). This study exclusively used female mice to model TNBC in women only.

### Cell lines

The *Trp53*-null TNBC GEMMs were previously generated by transplantation of *Trp53*-deleted donor mammary epithelium into the cleared mammary fat pad of syngeneic BALB/c hosts (10713689) these gave rise to re-transplantable heterogeneous mammary tumor TNBC cell lines. TNBC cell lines include T12 (BALB/c and Hsd:Athymic Nude-*Foxn1<sup>nu</sup>*), 2151R (BALB/c), T11 (BALB/c), 2336R (BALB/c) and 2208L (BALB/c). Established cells were cultured in DMEM/F-12 medium (Thermo Fisher Scientific, 11330032) supplemented with 10% fetal bovine serum (FBS) (GenDEPOT, F0900-050), 5 µg/mL insulin (Sigma-Aldrich, I-5500), 1 µg/mL hydrocortisone (Sigma-Aldrich, H0888), 10 ng/mL epidermal growth factor (Sigma-Aldrich, SRP3196), and 1x Antibiotic-Antimycotic (Thermo Fisher Scientific, 15240062). All cells were tested to be free of mycoplasma contaminants using the Universal Mycoplasma Detection Kit (ATCC, 30-1012K). Established cell lines were then transplanted into BALB/c mice, these tumors were then banked down for long-term storage in FBS + 10% DMSO.

### Tumor transplantation

Prior to tumor transplantation and surgery, tumors were rapidly thawed and washed in PBS to remove residual DMSO. Briefly, tumor tissues were transplanted into the fourth mammary fat pad of 6- to 8-week-old female BALB/c from Inotiv (strain 047) mice or athymic nude mice from Inotiv (strain 069), respectively. When tumors reached an

average size of 70 to 150 mm<sup>3</sup>, mice were randomized. Tumor volume and body weight were measured every 3 to 7 days, volume was calculated as (length × width<sup>2</sup>)/2. The ethical endpoint was met when the tumor reached a volume of 1500 mm<sup>3</sup>. Investigators were not blinded to the group assignment.

### **Tail vein (TV) injection and portal vein (PV) injection**

For experimental metastases, freshly digested tumor cells were prepared from T12 tumor tissues. T12 tumors were transplanted into the mammary gland of a WT BALB/c mouse as described above. When the tumor reached approximately 1 cm in diameter, the tumor was harvested and processed into a single-cell suspension. Briefly, tumors were digested with 1 mg/mL collagenase type I (Sigma-Aldrich, 11088793001) and 1 µg/mL DNase (Sigma-Aldrich, 11284932001) for 2 hours at 37°C on a shaker. Three rounds of rapid centrifugation were performed to enrich tumor cells by isolating stromal cells. The cell pellets were then trypsinized, counted, and filtered into single cell suspension. Established lung metastases were generated via TV injection of 30,000 unlabeled freshly dissociated cells suspended in 200 µL of PBS into each 8- to 10-week-old female BALB/c mice. PV injections were performed following established protocols (56). Briefly, after anesthetizing the animals and sterilizing the surgical site, a small incision (1-inch) was made between the median and sagittal planes on the left side of the mouse. 3,000 (unlabeled) freshly digested tumor cells, suspended in 5 µL of PBS were then slowly injected into the portal vein using a 32-gauge needle (Hamilton). A hemostatic gauze with gentle pressure will be placed at the injection site to manage the bleeding before closing the wound. The ethical endpoint was met when the mice lost approximately 20% body weight or if the mice exhibited ruffled fur and or hunched posture. To ensure successful generation of lung or liver metastases, several mice were injected with 60 mg/kg BrdU (Sigma-Aldrich, B-5002) 2 h prior to sacrifice to identify proliferative cells. Mice that experience lung and or liver metastases rapidly decline, thus body weight was measured every 3 to 7 days. The ethical endpoint was met when mice either lost approximately 20% body weight or display poor body condition.

### ***In vivo treatments***

Anti-CSF-1R monoclonal antibody, SNDX-ms6352 was donated by Syndax Pharmaceuticals, Inc. and was administered via i.p. injection weekly for 4 weeks. Per Syndax recommendation, mice were administered an initial dose of 40 mg/kg was first administered, followed by 20 mg/kg for the remaining three doses. Control mice were injected with equal volume of InVivoMab mouse IgG1 isotype control (Bio X Cell, BE0083). Cyclophosphamide (Sigma-Aldrich, PHR1404-1G) was resuspended in sterile PBS (Lonza). Mice were injected i.p. at the concentration of 100 mg/kg, once a week for up to four weeks. Control mice were injected with the same volume of sterile PBS. For ICB treatment, mice were administered RecombiMab anti-mouse PD1 (BioXcell, CD279, CP151) and RecombiMAb anti-mouse IgG2a isotype (BioXcell, CP150) 200 µg per mouse every three days via i.p. injection. *In vivo* antibodies were diluted with InVivoPure pH 7.0 Dilution Buffer (BioXCell, IP0070).

### **Tumor associated macrophage isolation and *in vitro* treatments**

TAMs were directly isolated from T12 primary mammary tumors transplanted in female BALB/c mice using mouse CD11b positive selection beads (STEMCELL Technologies, 18970). Briefly primary tumors were harvested and processed into a single-cell suspension as previously described. Following quick centrifugation, the stromal compartment (macrophage enriched) was utilized. Stromal cells were resuspended in DMEM/F12 medium (Thermo Fisher Scientific, 11330032) with 2% FBS. Stromal cells were then filtered, counted and isolated using the EasySep Magnet (STEMCELL Technologies, 18000). TAMs were then cultured in the appropriate TAM medium consisting of RPMI-1640, no glutamine (Thermo Fisher Scientific, 21870076) 20% FBS, 200 µM L-glutamine (Thermo Fisher Scientific, 25030081), 100 µM sodium pyruvate (Thermo Fisher Scientific, 11360070), 55 µM 2-mercaptoethanol (Thermo Fisher Scientific, 21-985-023), 10 ng/ml mouse M-CSF (Biolegend, 576406) and MEM Non-Essential Amino Acids Solution (Thermo Fisher Scientific, 11140050). Non-adherent cells were washed away post 2h incubation with PBS. Subsequently, 500,000 TAMs were cultured in 6 well-plates and treated with increasing concentration of SNDX-ms6352

(Syndax Pharmaceuticals, Inc.) or IgG1 isotype control (Bio X Cell, BE0083). TAM growth was monitored using the IncuCyte S3 Live-Cell Analysis System.

### **Immunoblotting**

For immunoblotting, TAMs were detached from the culture dish and lysed using RIPA buffer (10mM Tris-HCl, pH 8.0, 1mM EDTA, 0.5mM EGTA, 1% Triton X100, 0.1% Sodium Deoxycholate, 0.1% SDS, 140mM NaCl). BCA assay (Pierce BCA Protein Assay Kit, Thermo Fisher Scientific, 23225) was used to determine protein concentration. Equal amount of protein was separated by SDS-PAGE using Mini-Protean TGX polyacrylamide gels (Bio-Rad). Subsequently, proteins were transferred from the gel to the Immobilon PVDF membranes (Millipore, IPVH00010). Following a 1h blocking step with 5% BSA, the membranes were incubated with anti-CSF-1R (Cell Signaling TECHNOLOGY, 43390) and anti-CD206/MRC1 (Cell Signaling Technology, 24595) overnight at 4°C with primary antibodies. The following day, membranes were probed with secondary HRP antibodies Goat anti-Rabbit IgG (Invitrogen, 31460) and scanned using the Amersham Imager 600 system.

### **Immunohistochemistry and immunofluorescence**

Primary tumors, mammary glands, lung and liver tissues were fixed in 4% paraformaldehyde for 24h at 4°C and subsequently changed to 70% EtOH prior to paraffinization and embedding. For lung and liver metastases, 5-6 serial sections (5- $\mu$ m per section) were collected every 150  $\mu$ m.

For H&E staining, tissues were deparaffinized and rehydrated and stained Harris Hematoxylin (Poly Scientific, S176). For IHC analysis sections were first deparaffinized and rehydrated, antigen retrieval was conducted using citrate buffer (pH 6.0) placed on a steamer for 30 min. Endogenous peroxidase was performed using 3% H<sub>2</sub>O<sub>2</sub> (Thermo Fisher Scientific, H323-500) in PBS for 10 min. Sections were then incubated in the appropriate blocking buffer containing 3% BSA (Sigma-Aldrich, A7906) and 5% goat

serum (Sigma-Aldrich, G9023) in PBS for 1h at room temperature and incubated in the respective primary antibodies overnight at 4°C. For IHC the following primary antibodies were utilized: anti-F4/80 (Cell Signaling Technology, 70076; 1:500), anti-S100A8 (R&D Systems, MAB3059; 1:5000), anti-CD8α (Cell Signaling Technology, 98941; 1:500) and anti-CD4 (Abcam, ab183685 1:400). Biotin-conjugated secondary antibodies, anti-rabbit (Vector Laboratories, PI-1000-1) or anti-rat (Vector Laboratories, PI-9400-1) were incubated for 1h at room temperature. VECTASTAIN Elite ABC HRP Reagent (Vector Laboratories, PK7100) was used to amplify signal according to the manufacturer's protocol and developed with ImmPACT DAB peroxidase substrate (Vector Laboratories, sk-4105). The slides were counterstained with Haris Hematoxylin (Poly Scientific, S212A). IHC and H&E-stained slides were imaged using the Olympus BX40 light microscope and MPX-5C pro low-light camera at x20 magnification or scanned with the Aperio ImageScope (Leica Biosystems) and analyzed using the Aperio ImageScope software (v12.3.3.5048). At least three representative images of primary tumor, lung and liver metastases were acquired for analysis.

For immunofluorescence analysis deparaffinized and rehydrated slides were subjected to antigen retrieval using Tris-EDTA antigen retrieval buffer (10 mM Tris, 1 mM EDTA, 0.05% Tween 20, pH 9.0). The following primary antibodies were incubated overnight at 4°C: anti-F4/80 (Cell Signaling Technology, 70076; 1:500), anti-S100A8 (R&D Systems, MAB3059; 1:5000), anti-BrdU (1:1000; Abcam, ab6326), anti-cleaved caspase 3 (Cell Signaling Technology, 9661, 1:1000), anti-CD8α (Cell Signaling Technology, 98941; 1:500), anti-CD20 (Cell Signaling Technology, 70168; 1:500), anti-CSF-1R/M-CSF-R (Cell Signaling Technology, 43390, 1:500) and anti-CD8α (eBioscience, 14-0081-82; 1:500). For immunofluorescence staining of actin and F4/80 in TAMs, the isolated TAMs were first cultured in 8-well chamber cell culture slides (Corning, 354108) 48h after treatment, fixed in 4% paraformaldehyde for 15 min and permeabilized with 0.5% Triton X-100 followed by overnight blocking in 3% BSA at 4°C. Following several washes with PBS both slide and cells were incubated in the appropriate conjugated secondary antibody (Alexa Fluor 488/594/647) for 1h at room temperature. The slides were counterstained with DAPI (Invitrogen™, R37606) for 20 min at room temperature and mounted using aqua-Poly/Mount (Fisher Scientific, NC9439247). Immunofluorescent images were taken

using the Nikon A1-Rs confocal microscope at x20 and x40 magnification and quantified using the Fiji software.

### Cytokine profiling

Snap-frozen tumor tissues from *in vivo* treatments were thawed and homogenized using zirconium beads in the BeadBlaster 24 Microtube Homogenizer. The tissues were homogenized in the T-PER Tissue Protein Extraction Reagent (Thermo Fisher Scientific, 78510) with EDTA-free Protease Inhibitor Cocktail. The BCA Protein Assay Kit was utilized to determine protein concentrations. Equal amount of homogenate was measured and diluted 2-fold in PBS. Samples were profiled using the Mouse Cytokine/Chemokine 44-Plex Discovery Assay Array (Eve Technologies Corp., MD44).

### Imaging mass cytometry (IMC)

Formalin-fixed paraffin-embedded tissues were deparaffinized in fresh 100% Xylene three times for 5 min and rehydrated in a series of ethanol (100%, 100%, 95%, 80% 70%) 5 min each. Washed with deionized water for 5 min with gentle agitation. Antigen retrieval was performed using Tris-EDTA (pH 9.0) (eBioscience, 00-4956-58), incubated at 95°C for 30 min in a steamer and allowed to cool in the same solution for 30 min. The slides were then washed with deionized water for 10 min and subsequently blocked with 3% BSA in PBS for 1h at room temperature in a hydration chamber. The slides were then incubated with the respective metal tagged antibody cocktail overnight at 4°C in a hydration chamber. The slides were then washed 2 times in PBS-T for 5 min and 2 more times in PBS prior to being incubated with 0.125 µm of Interculator-Ir (Standard Biotools) in PBS for 30 min at room temperature in a hydration chamber. The slides were then washed in deionized water for 5 min and left to air dry for 20 min at room temperature.

Stained and dried tissue slides were loaded into the Hyperion tissue imager and ablated by a high energy UV laser beam 1mm<sup>2</sup>/pixel at 200Hz. The ablated material is transported by argon gas into the plasma of the mass cytometer, where first atomized/ionized, then

low-molecules ions filtered and analyzed in the time-of-flight (TOF) mass spectrometer. Multiplexing Image data with spatial information are reconstructed and saved in MCD. Format for down-stream analysis. Cell-level image quality-control is first evaluated with the MCD viewer software provided by Standard Biotools. The full resolution IMC images (10X) in MCD. format is added to the Visiopharm® database and color-adjusted for best visualization for nuclear detection and segmentation. Cell segmentation is performed using DNA signal to find the nuclei followed by Visiopharm® designated algorithms including polynomial blobs to refine the separation of cells. Cellular phenotyping is then performed, and spatial data (Nearest Neighbor) calculated using Visiopharm® designated Phenoplex Guided Workflow. Analyzed data with all cells and their phenotypes were exported to TSV. file for further analysis. TSV files were first processed in R using FlowSOM, flowCore and SingleCellExperiment packages in preparation for further analyses using the CATALYST package (version 1.14.0, <https://github.com/HelenaLC/CATALYST>). The markers included in the analyses were Pan-CK, CD44, F4/80, S100A8, S100A9, PD-L1, Ki67, CD4, CD8a, Vimentin and PD-1. Clustering was performed using the cluster (CATALYST) function (maxK = 20). Cluster annotations were performed manually (neutrophils: S100A8/S100A9; macrophages: F4/80; tumor cells: Vimentin/CD44). The clusters which lacked the expression of these markers were labeled as unidentified. Dimension reduction by TSNE was performed and plotted using runDR (CATALYST) function using 5000 cells per sample. Clusters were merged based on annotations using the mergeClusters (CATALYST) function. All plots were generated using the CATALYST package.

For cluster analysis IMC markers were divided into those that are expressed in the nucleus, such as DNA (channels 191Ir and 193Ir), Ki67, Ly6G, B220, F480, S100A8/9, and those that are expressed in the cell membrane, such as CD4, CD8a, CD11b, CD11c, CD44, CD62L, CD68. Composite images were generated for nucleus and cell membrane. Next, a combined image of the cells (nucleus + cell membrane) was generated for the purpose of cell segmentations. To perform cell segmentation, we first converted each image to grayscale, then highlighted in-cell pixels using the Threshold menu option in ImageJ. Approximately 40-55% of pixels per image were highlighted as red (i.e., in-cell pixels). With these in-cell pixels highlighted as red on the screen, we next used “Find

Maxima” function, followed by setting output to “Segmented Particles” in ImageJ to create black segmented cell masks. Results were outputted to the ROI manager and subsequently saved as a ROISet.zip file. We next quantified the total intensities of pixels per protein marker per cell (given the available cell masks created from segmentation). Eventually, this created a cell-by-protein matrix for all segmented single-cells and protein markers in each image. On this matrix, we performed log-transformation, followed by row-wise z-scoring (across cells), and column-wise z-scoring (across markers). The resulting matrix was subject to K-means clustering with a high number of random starts (nstart=100,000) for reliable centroid generation was used. K-means promoted greater tolerance for variation and noise in data processing, were less sensitive and more robust to outlier expression, and avoided the generation of ROI -specific clusters. 20 clusters were determined showing robust cluster-specific expression. Differentially expressed proteins across clusters were then determined by performing all one-vs-one comparisons, and then setting a threshold for significance. This threshold was set at 17/19, meaning that a protein is deemed to be differentially expressed for a cluster if the protein is significant in 17 out of 19 one-vs-one comparisons between that cluster and the rest. After that, each cluster was named by the list of differential markers expressed in the cluster.

Image acquisition was performed using the available histoCAT web (<http://github.com/BodenmillerGroup/histocat-web>) software. The antibody panel was designed to study the TIME within metastatic lesions; thus we included markers to identify tumor cells (PanCK, Vimentin, CD44), proliferation marker (Ki-67), lymphocytes (CD8, CD4, FoxP3, CD127, CD62L, B220), Monocytes (F4/80, S100A8, S100A9, Ly6C, Ly6G, CD163, CD11c, CD86) and the checkpoint markers (PD-L1, PD-1). Multiple iridium staining makers (191Ir, 193Ir) were used for nuclei detection. The antibody panel was designed from our previous study (15) and literature search.

For antibody validation a separate tissue microarray (TMA) was generated using normal spleen, normal lung, lung metastases and primary tumor tissues from paraffin embedded blocks, sectioned at 5 µm. Each specific region of the slide contained the four varying tissues and was separated using a hydrophobic PAP pen. The TMA was generated by the Human Tissue Acquisition and Pathology Core and inspected by a pathologist to

assess tissues. Four different antibody cocktail dilutions were then tested, each cocktail contained 23 different antibodies. Multiple antigen retrieval buffers were simultaneously tested with each cocktail dilution, including citrate buffer (pH 6.0) and IHC Antigen Retrieval Solution (10 mM Tris, 1 mM EDTA, pH 9.0) (eBioscience, 00-4956-58). The different cocktail groups were obtained analyzed and validated in conjunction with The Cytometry and Cell Sorting Core (CCSC) at Baylor College of Medicine (BCM).

### **Flow cytometry**

For the enrichment of stromal cells, single cell suspensions were generated following the digestion of tumor tissues with collagenase as previously described. Briefly, stromal cells were collected following quick centrifugations and incubated in RBC lysis buffer (BioLegend, 420301), the cells were resuspended following lysis inactivation, counted and filtered PBS + 2% FBS. Prior to blocking, anti-mouse CD16/CD32 antibody (BioLegend, 101320) 1 million cells were stained with Live/Dead Fixable Yellow (Invitrogen™, L34968; 1:800). Stromal cells were incubated with the cell surface F4/80-APC (BioLegend, 123115). Following antibody staining, the resuspended cells (PBS) were analyzed using the Attune NxT flow cytometer at the FACS and CCSC at BCM. Compensation and further analyses were performed using the FlowJo v10 software.

### **Single-cell RNA-sequencing (scRNA-seq)**

For scRNA-seq, all mice received the final doses 24h prior to euthanasia. Single cell suspensions were processed as previously described and pooled from 3 mice per treatment. Only viable cells were used for single cell analysis as such, isolated single cell suspensions were first stained with Ghost Dye UV 450 (Tonbo Biosciences, 13-0868) for 10 min and sorted via FACS to isolate viable cells. Briefly, primary tumor cells were harvested and resuspended in RBC Lysis Buffer (BioLegend, Inc., 420301) and passed through a 70- µm strainer. Viable single cell suspensions were tagged with 3' CellPlex barcoding oligos (10X Genomics, PN-1000262) and were quickly subjected for scRNA-seq library preparation by the Single Cell Genomics Core at BCM. Single-cell libraries

were prepared following the Chromium Single Cell Gene Expression 3' v3.1 kit encompassing the multiplex capture CMO barcoding kit (10x Genomics, PN-1000262). Next generation library sequencing was performed using the NovaSeq 6000 (Illumina) following quality control check.

Using the raw sequencing data, alignment, read counts and sample demultiplexing was performed using the CellRanger multi (v7.2.0) pipeline. The barcode assignment confidence was set to 0.8 to capture a larger number of cells for downstream processing. scRNA-seq was analyzed using the Seurat (v4.4.0) package in R (R version 4.3.1; <https://github.com/satijalab/seurat>). Only cells with less than 6000 and more than 200 read counts were utilized for downstream analysis to accommodate for quality control. Cells with more than 10% mitochondrial ratio and over 1000 UMI were removed. Individual datasets were batch-corrected and integrated using the IntegrateData function.

### **Adoptive T cell transfer**

T cells were directly isolated from the spleens of female BALB/c mice that were bearing T12 liver metastases and had been previously treated for 56 days and rejected tumor cell rechallenge. Briefly, spleens were first dissociated using the Spleen Dissociation Medium (STEMCELL Technologies, 07915). Splenocytes were isolated using the EasySEP Mouse T Cell Isolation Kit (STEMCELL Technologies, 19851), negative selection was performed using the EasySep Magnet (STEMCELL Technologies, 18000). T cells were then resuspended in PBS, counted and directly transferred into T12 primary tumor bearing female BALB/c via TV injection and treated with RecombiMab anti-mouse PD1 (BioXcell, CD279, CP151) or RecombiMAb anti-mouse IgG2a isotype (BioXcell, CP150) 200 µg per mouse.

### **Radiopharmaceuticals (FDG) and Small-Animal PET-CT**

Fluorine-18 labeled fluoroxyglucose (18F-FDG), purchased from Sofie, (Houston, TX). All CT and PET images were acquired using an Inveon scanner (Siemens AG, Knoxville,

TN). The mice were injected with 11.1 MBq (300  $\mu$ Ci) of 18F-FDG radiotracer at any given time. To identify metastases or measure tumor metabolic activities, 18F-FDG injected intra peritoneal. Before 18F-FDG administration, the mice were fasted for approximately 12 hours. PET and CT performed one hour after injection of FDG. During imaging, a respiratory pad was placed under the abdomen of the animal to monitor respiration (Bovet, Newark, NJ). Mice were anesthetized with isoflurane gas (1-3%) mixed with oxygen at a flow rate of 0.5-1 L/minute and adjusted accordingly during imaging to maintain normal breathing rates. A CT scan acquired with the following specifications: 220 acquired projections each projection was 290 ms with x-ray tube voltage and current set at 60 kVp and 500  $\mu$ A, respectively. A 40-minute PET scan immediately acquired after CT. The PET scans were reconstructed using OSEM3D reconstruction method and co-registered to the CT scan for attenuation correction.

## PET Image Analysis

The PET images were quantified using Inveon Research Workspace IRW (IRW, Siemens AG, Knoxville, TN). Using the reconstructed PET scan, lung and liver manually selected to form regions of interest (ROI) on the PET-CT images. Activity measurements (Bq/cm<sup>3</sup>) were divided by the decay-corrected injected dose (Bq) and multiplied by 100 to calculate tissue uptake index represented as percentage injected dose per gram of tissue. The data represented as standardized uptake value (SUV) normalized to body weight.

## AURORA data analysis

The batch-corrected and normal tissue-adjusted gene expression and expression signature data were obtained from the AURORA USA clinical study (**GSE209998**) (11). For primary figures the data were filtered to contain only triple-negative primary tumors, lung metastases, and liver metastases (**Supplementary tables S16 and S17**). Differential gene expression/expression signature analyses were performed using the limma package. Patient IDs were treated as a corresponding variable. For all multiple comparisons, p-values were adjusted using the Benjamini-Hochberg method. Gene set

enrichment analyses were performed using the fgsea package. Gene sets with adjusted p-values < 0.05 were considered significant.

## Statistics

Detailed statistical methods are outlined within the figure legends of this manuscript, depicting the number of animals or independent replicates, along with the statistical tests used. For pairwise comparisons or comparisons of 3 or more groups ordinary one-way ANOVA was used. Two-way ANOVA and Šidák's multiple-comparison test were used for analyzing tumor volume changes, log (fold changes) of tumor volume and Tukey's multiple-comparison test were used for body weight changes over time. For Kaplan-Meier curves, the log-rank test was performed. For comparison between 2 groups, unpaired, 2-tailed Student's t test was used. Paired t test was used for PET/CT analysis. The above-mentioned statistics were calculated using GraphPad Prism Version 10.3.0. For scRNA-seq, statistical analyses were performed in R. Log<sub>2</sub> (fold change) greater than 0.5 or less than -0.05, and an adjusted *P* value of less than 0.01 was considered significant in differential gene expression analyses. An adjusted *P* value of less than 0.05 was considered significant in GO pathway enrichment analyses. For IMC, the statistical analyses of differential expression were performed using the multcomp and diffcyt packages with all clusters merged. Contrast matrices were created for each comparison between two conditions. *P*-values were generated using diffcyt function (type of analysis, DS; method for DS testing, diffcyt-DS-limma). *P*-values were then adjusted using the Benjamini-Hochberg method.

## Data Availability

Raw and analyzed scRNA-seq data has been deposited in the NCBI GEO database (accession number: GSE292908). Detailed information regarding the antibodies used for IMC is provided in **Supplementary table S18**, IMC single cell analysis provided in **Supplementary tables S19-21**. All unique/stable reagents generated in this study are available from the Lead Contact following a completed Materials Transfer Agreement

(MTA). Further information and requests for resources and reagents should be directed to and will be fulfilled by the Lead Contact, Jeffrey M. Rosen ([jrosen@bcm.edu](mailto:jrosen@bcm.edu)). All illustrations were created with BioRender.

## AUTHOR CONTRIBUTIONS

D.A.P. conceptualized and designed the study, conducted the experiments, analyzed the data, and wrote the manuscript. X.Y., F.L., H.L.C., W.B. and Q.Z. provided bioinformatics support. C.Z., S.J.C., N.L., C.V.O., O.P. conducted experiments and analyzed data. W.W and P.P analyzed imaging mass cytometry experiments. A.J.S. and N.Z. designed the flow cytometry experiments and analyzed the data. P.S. and M.W.G. conducted PET/CT scans and analyzed the data. C.M.P. provided bioinformatics support and edited the manuscript. X.H.-F.Z. and J.M.R. conceived and supervised the study and edited the manuscript.

## ACKNOWLEDGEMENTS

We are grateful for the suggestions from both the Zhang and Rosen laboratory members. We thank Peter Ordentlich from Syndax for providing SNDX-ms6352 and Dr. Patricia Castro from the Human Tissue Acquisition and Pathology Core at BCM for IMC antibody validation. D.A.P. is supported by the American Cancer Society Postdoctoral Fellowship (PF-22-163-01-MM) and NIGMS MOSAIC (1K99GM155594-01). A.J.S. is supported by Susan G Komen (SAC232150). N.Z. is supported by Cancer Prevention and Research Institute of Texas (CPRIT) (RP220468). J.M.R. is supported by NIH (R01CA016303-46 and R01CA148761-13) and Susan G Komen (SAC232150). X. H.-F.Z. is supported by US Department of Defense (DAMD W81XWH-16-1-0073 and DAMD W81XWH-20-1-0375), NIH (R01CA183878, R01CA227904, R01CA221946, and R01CA251950), the Breast Cancer Research Foundation, and McNair Foundation. This project was supported by the Cytometry and Cell Sorting Core at Baylor College of Medicine with funding from the CPRIT Core Facility Support Award (CPRIT-RP180672), the NIH (CA125123 and RR024574) and the assistance of Joel M. Sederstrom. The scRNA-seq experiments were

supported by the Single Cell Genomics Core at BCM, which is partially supported by NIH (S10OD025240) and CPRIT (RP200504). The Integrated Microscopy core supported by NIH (DK56338, CA125123, ES030285), and CPRIT (RP150578, RP170719). We thank the Pathology Core of Lester and Sue Smith Breast Center at BCM for tissue sectioning.

## AUTHOR'S DISCLOSURE

C.M.P. is an equity stockholder of and consultant for BioClassifier LLC. C.M.P. is also listed as an inventor on a patent application (US9631239B2) for the Breast PAM50 Subtyping assay (not related to this work).

## FIGURE LEGENDS

**Figure 1. CSF-1R inhibition coupled with LDMC leads to a durable response in primary macrophage enriched TNBC pre-clinical GEMMs.** (A) Imaging mass cytometry analysis depicting differential expression of immune (F4/80, S100A8/9, CD8, FoxP3), EMT (Vimentin), proliferation (Ki67) and exhaustion (PD-L1) markers from different p53-/ GEMMs. GEMMs include the claudin-low (T12, 2151R and T11), Basal-like (2336R) and luminal-like (2208L). Representative images are from a single ROI taken from a tissue microarray (TMA). (B) Bar plots identify different cluster id's including macrophages, neutrophils and various tumor cells within the different models. (C) Schematic representation of treatment regimen. Tumor chunks were first transplanted into female Balb/c mice, once palpable, mice were randomized and considered to be day 0. IgG control, CTX and SNDX-ms6352 were administered i.p. once a week for 4 weeks. All treatments were stopped at day 28 and recurrence was assessed from 56-70 days. (D) Kaplan-Meier survival curves following IgG Control, SNDX-ms6352, CTX and CTX+SNDX-ms6352 in multiple TNBC pre-clinical GEMMs. Statistical analysis performed using Log-rank (Mantel-cox) test ( $n = 5-8$  mice per treatment). (E) Schematic representation of tumor cell rechallenge experiment. Post tumor chunk transplantation and treatment cessation post 28 days, CR mice were rechallenged with 1,000 freshly dissociated tumor cells in the contralateral mammary gland. (F) Tumor volume of weight matched control (naïve) mice and CR mice rechallenged with T12 tumor cells. Significance determined by Two-way ANOVA and Šidák's multiple comparisons test ( $n = 5$  control mice and  $n = 4$  CR mice). (G) UMAP visualization post 10-day (short-term) treatment of IgG Control, CTX, SNDX-ms6352 or CTX+SNDX-ms6352 in T12 and 2151R primary tumors ( $n = 3$  mice per treatment). (H) Gene ontology analysis of residual inflammatory macrophage phenotypes. (I) Gene ontology analysis of residual lipid-associated macrophage phenotypes. (J) Circle plot demonstrating intercellular cell-cell communication and disruption of the CSF signaling network between immune and tumor cells within each treatment in T12 and 2151R primary tumors. (K) M-CSF, IL-17, IL-5 and INF- $\gamma$  plasma cytokine levels from tumor bearing mice following each treatment in T12 primary tumors. Significance determined by ordinary one-way ANOVA and Tukey's

multiple comparisons test ( $n = 3$  mice per treatment). Data shown as mean  $\pm$ SEM. For all panels \* $P < 0.05$ ; \*\* $P < 0.01$ ; \*\*\*  $P < 0.001$ ; \*\*\*\* $P < 0.0001$ .

**Figure 2. Combination treatment leads to ITH driven PD-1/PD-L1 axis in metastatic lung metastases.** (A) Schematic illustration of treatment regimen. Tumor cells are first injected via TV into female Balb/c mice. Post 12-day TV injection the mice were randomized and considered to be day 0. IgG control, CTX and SNDX-ms6352 were administered i.p. once a week for 4 weeks. All treatments were stopped at day 28 and recurrence was assessed at day 56. (B) Representative H&E and immunofluorescence staining of BrdU in lung metastases 12 days post TV injections. (C) Kaplan-Meier survival curves following IgG Control, SNDX-ms6352, CTX and CTX+SNDX-ms6352 in T12 with established lung metastases. Statistical analysis was performed using the Log-rank (Mantel-cox) test ( $n = 6$  mice per treatment). (D) Mouse body weight (g) following IgG Control, SNDX-ms6352, CTX and CTX+SNDX-ms6352 in T12 established lung metastases. Significance determined by Two-way ANOVA and Tukey's multiple comparisons test ( $n = 6$  mice per treatment). (E) Schematic illustration of IgG control mice at day 21 and CTX+SNDX-ms6352 treated mice at day 56, subjected for IMC analysis to study the metastatic TIME. (F) IMC analysis post CTX+SNDX-ms6352 treated T12 GEMMs at day 56 from independent lung tissues. Representative markers included Vimentin, Pan-CK, CD44, S100A8/9, PD-L1, PD-1, Ki67, and 191ir (DAPI). (G) TSNE plot visualization of tumor cells, PD-L1, PD-1 and Pan-CK in IgG control and CTX+SNDX-ms6352 treated. (H) TSNE plot visualization of PD-L1 and PD-1 expression in IgG control and CTX+SNDX-ms6352 treated. (I) Schematic illustration of tumor cell re-challenge. Mice that were deemed as complete responders (CR) at day 56 were re-challenged by injecting 1,000 unlabeled cells into the mammary gland (primary site of tumor origin). Metastatic TIME was assessed via IMC. Data shown as mean  $\pm$ SEM. For all panels \* $P < 0.05$ ; \*\* $P < 0.01$ ; \*\*\*  $P < 0.001$ ; \*\*\*\* $P < 0.0001$ .

**Figure 3. Addition of anti-PD1 reshapes the landscape of the metastatic TIME leading to the proximity of B-, T cells and neutrophils and a therapeutic response in established lung metastases.** (A) Schematic illustration of short-term treatment

regimen. T12 tumor cells are first injected via TV into female Balb/c mice. Post 19-day TV injection the mice were randomized and considered to be day 0. IgG control, CTX and SNDX-ms6352 were administered i.p. at day 0 and day 7, anti-PD1 and its IgG2a isotype control were administered every 2 days. (B) Mouse body weight (g) following short-term treatment of IgG Control, SNDX-ms6352, CTX, CTX+SNDX-ms6352 and CTX+SNDX-ms6352+aPD1 in T12 GEMMs with established lung metastases. Statistical analysis was performed using Two-way ANOVA and Tukey's multiple comparisons test ( $n = 5$  mice per treatment). (C) Quantification of lung metastases post short-term treatment. Serial sectioning was performed to collect a total of 10 sections for each sample. Metastases with sizes of <1 mm, 1-3 mm, 3-5 mm, and >5 mm were assigned scores of 1, 2, 3, and 4, respectively. Significance determined by Two-way ANOVA and Tukey's multiple comparisons test. (D) Representative H&E staining of lung metastases at day 7 post IgG control, SNDX-ms6352, CTX, CTX+SNDX-ms6352 and CTX+SNDX-ms6352+aPD1 treatments ( $n = 5$  mice per treatment). (E) Imaging mass cytometry analysis post IgG control, SNDX-ms6352, CTX, CTX+SNDX-ms6352 and CTX+SNDX-ms6352+aPD1 treated T12 GEMMs at day 7. Clustered and individual channels include Vimentin, CD44, F4/80, S100A8, PD-L1, Ki67, and 191ir (DAPI) markers. (F) Median distance of immune cells from tumor cells post IgG control, SNDX-ms6352, CTX, CTX+SNDX-ms6352 and CTX+SNDX-ms6352+aPD1 treated T12 GEMMs at day 7, distance analysis is representative from IMC analysis of individual channels CD8, CD4, S100A8/9 and F4/80. Significance was determined using Two-way ANOVA and Tukey's multiple comparisons tests ( $n = 3$  ROI). (G) Median expression levels of the exhaustion markers PD-L1 and PD-1 post IgG control, SNDX-ms6352, CTX, CTX+SNDX-ms6352 and CTX+SNDX-ms6352+aPD1 treated T12 GEMMs at day 7.  $P$ -values were generated using diffcyt function (type of analysis, DS; method for DS testing, diffcyt-DS-limma).  $P$ -values were then adjusted using the Benjamini-Hochberg method ( $n = 3$  ROI). (H) Illustration depicting pro-tumor immunosuppressed and anti-tumor, tumor killing phenotypes. Phenotypes are representative of the proximity between TAMs, CD4, CD8, S100A/9 Neutrophils within tumor cells. Data shown as mean  $\pm$ SEM. For all panels \* $P < 0.05$ ; \*\* $P < 0.01$ ; \*\*\*  $P < 0.001$ ; \*\*\*\* $P < 0.0001$ .

**Figure 4. Triple combination treatment leads to long-term durable response of established lung metastases.** (A) Schematic illustration of long-term treatment regimen. T12 tumor cells are first injected via TV into female Balb/c mice. Post 12-day TV injection the mice were randomized and considered to be day 0. IgG control, CTX, SNDX-ms6352, CTX+SNDX-ms6352 and CTX+SNDX-ms6352+aPD1 were administered i.p. once a week for 4 weeks, anti-PD-1 and its IgG2a isotype control were administered every 3 days. Treatments were stopped at day 28 and recurrence was assessed at day 56, except for the group that continued to receive a maintenance does (M. dose) of anti-PD-1. (B) Kaplan-Meier survival curves following IgG Control, SNDX-ms6352, CTX, CTX+SNDX-ms6352 and CTX+SNDX-ms6352+aPD1 +/- M. dose in T12 GEMMs with established lung metastases. Statistical analysis was performed using the Log-rank (Mantel-cox) test ( $n = 5-7$  mice per treatment). (C) Mouse body weight (g) following IgG Control, SNDX-ms6352, CTX, CTX+SNDX-ms6352 and CTX+SNDX-ms6352+aPD1 +/- (M. dose) in T12 GEMMs with established lung metastases. Significance was determined by Two-way ANOVA and Tukey's multiple comparisons test ( $n = 5-7$  mice per treatment). (D) Tumor volume of weight matched control (naïve) mice and CR mice rechallenged with T12 tumor cells. Significance was determined by two-way ANOVA and Šidák's multiple comparisons test ( $n = 5$  control mice and  $n = 5$  CR mice). (E) Double immunofluorescence (IF) staining of CSF-1R, BrdU, CD20, CD8 and DAPI in T12 GEMMs with established lung metastases treated with CTX+SNDX-ms6352+aPD-1 (Representative image of  $n = 5$  mice). (F) Quantification of mean fluorescence intensity (MFI) staining of CSF-1R, BrdU, CD20 and CD8 in T12 mice with established lung metastases following IgG control, CTX, SNDX-ms6352, CTX+SNDX-ms6352 and CTX+SNDX-ms6352+aPD-1. Significance was determined by Two-way ANOVA and Tukey's multiple comparisons test ( $n = 5$  mice per treatment). Data shown as mean  $\pm$ SEM. For all panels \* $P < 0.05$ ; \*\* $P < 0.01$ ; \*\*\* $P < 0.001$ ; \*\*\*\* $P < 0.0001$ .

**Figure 5. Established T12 liver metastases present with an immunologically cold TIME.** (A) Schematic illustration of PV injection utilized to generate experimental liver metastases. (B) Representative H&E and IHC staining of F4/80, S100A8, CD8 and CD4 in T12 GEMMS bearing liver metastases post 15 days PV injections. (C) Representative H&E and IF staining of BrdU in liver metastases 15 days post T12 tumor cell PV injections.

(D) Schematic illustration of short-term treatment regimen. Tumor cells are first injected via PV into female Balb/c mice. Post 15-day PV injection the mice were randomized and considered to be day 0. IgG control, CTX and SNDX-ms6352 were administered i.p. at day 0 and day 7, anti-PD-1 and its IgG2a isotype control were administered every 2 days. (E) Mouse body weight (g) following short-term treatment of IgG control, SNDX-ms6352, CTX, CTX+SNDX-ms6352 and CTX+SNDX-ms6352+aPD-1 in T12 GEMMs with established liver metastases. Statistical analysis was performed using Two-way ANOVA and Tukey's multiple comparisons test ( $n = 3-5$  mice per treatment). (F) Quantification of liver metastases post short-term treatment. Serial sectioning was performed to collect a total of 10 sections for each sample. Metastases with sizes of <1 mm, 1-3 mm, 3-5 mm, and >5 mm were assigned scores of 1, 2, 3, and 4, respectively. Statistical analysis was performed using Two-way ANOVA and Tukey's multiple comparisons test as described above. (G) Representative H&E staining of liver metastases at day 7 post IgG control, SNDX-ms6352, CTX, CTX+SNDX-ms6352 and CTX+SNDX-ms6352+aPD-1 treatments ( $n = 3-5$  mice per treatment). (H) Heatmap depicting median expression levels of various immune (F4/80, S100A8/9, CD4 and CD8a), tumor (Pan-CK, CD44 and Vimentin), T-cell exhaustion (PD-L1 and PD-1) and proliferative (Ki67) markers following IgG control, SNDX-ms6352, CTX, CTX+SNDX-ms6352 and CTX+SNDX-ms6352+aPD-1 treated T12 liver metastases from IMC analysis.  $P$ -values were generated using diffcyt function (type of analysis, DS; method for DS testing, diffcyt-DS-limma).  $P$ -values were then adjusted using the Benjamini-Hochberg method ( $n = 3$  ROI). (I) Cumulative and individual marker (Vimentin, CD44, F4/80, S100A8, PD-L1 and Ki67) IMC analysis from IgG control, SNDX-ms6352, CTX, CTX+SNDX-ms6352 and CTX+SNDX-ms6352+aPD-1 treated liver metastases. Data shown as mean  $\pm$ SEM. For all panels \* $P < 0.05$ ; \*\* $P < 0.01$ ; \*\*\* $P < 0.001$ ; \*\*\*\* $P < 0.0001$ .

**Figure 6. An anti-PD-1 maintenance dose is necessary to generate long-term anti-tumor immunity and to eradicate established liver metastases.** (A) Schematic illustration of long-term treatment regimen. Tumor cells are first injected via PV into female Balb/c mice. Post 15-day PV injection the mice were randomized and considered to be day 0. IgG control, CTX, SNDX-ms6352, CTX+SNDX-ms6352 and CTX+SNDX-ms6352+aPD-1 were

administered i.p. once a week for 4 weeks, anti-PD-1 and its IgG2a isotype control were administered every 3 days. Treatments were stopped at day 28 and recurrence was assessed at day 56, except for the group that continued to receive a M. dose of anti-PD-1. (B) Coronal view of PET/CT scans depicting the uptake of 18-FDG in untreated T12 GEMMS with established liver metastases at day 15 post PV injections and post-treated follow up at day 56, (Representative image of  $n = 3$  mice per treatment). (C) Relative quantification of 18-FDG uptake in triple combination (m.dose) treated and untreated mice. Each dot represents the mean standard uptake values (meand SUV-bw) of 18-FDG. Significance was determined by paired t test ( $n = 3$  mice per treatment). (D) Kaplan-Meier survival curves following IgG control, SNDX-ms6352, CTX, CTX+SNDX-ms6352 and CTX+SNDX-ms6352+aPD-1 +/- M. dose in T12 GEMMs with established liver metastases. Statistical analysis using log-rank (Mantel-cox) test ( $n = 5-9$  mice per treatment). (E) Mouse body weight (g) following IgG control, SNDX-ms6352, CTX, CTX+SNDX-ms6352 and CTX+SNDX-ms6352+aPD1 +/- M. dose in T12 GEMMs established liver metastases. Significance was determined by Two-way ANOVA and Tukey's multiple comparisons test ( $n = 5-9$  mice per treatment). (F) Double IF staining of CD20, CD8 and DAPI in T12 GEMMS with established liver metastases treated with CTX+SNDX-ms6352+aPD-1 (Representative image of  $n = 5$  mice). (G) Quantification MFI staining of CSF-1R, BrdU, CD20 and CD8 in T12 mice with established liver metastases following IgG control, CTX, SNDX-ms6352, CTX+SNDX-ms6352 and CTX+SNDX-ms6352+aPD-1. Significance was determined by Two-way ANOVA with multiple comparisons test ( $n = 5$  mice per treatment). (H) Tumor volume of weight matched control (naïve) mice and CR mice rechallenged with T12 tumor cells. Significance determined by Two-way ANOVA and Šidák's multiple comparisons test, ( $n = 5$  control mice and  $n = 6$  CR mice). (I) Schematic illustration of adoptive T-cell transfer (ACT). Mice that completely rejected the tumor cell rechallenge were deemed to be CR.  $2.0 \times 10^6$  CD3 T-cells were then injected to T12 tumor bearing mice. To test T-cell exhaustion, the mice were also administered +/- aPD-1 and its isotype IgG control. (J) Tumor volume of mice bearing T12 tumors subjected to ACT and subsequently treated with IgG control and +/-aPD-1. Significance was determined by Two-way ANOVA with multiple comparisons test, ( $n = 4-8$  mice per treatment). (K) Representative images of isolated spleens from mice that were subjected to ACT and treated with IgG control and +/- aPD-1 (image is representative of  $n = 3$  mice per treatment). (L) Quantification of IHC staining of CD8 T-cells within the spleens of ACT transferred mice. Significance determined by ordinary one-way ANOVA, ( $n = 3$  mice per treatment). (M) Quantification of IHC staining

of CD8 T-cells within the tumors of ACT transferred mice. Significance determined by ordinary one-way ANOVA, ( $n = 3$  mice per treatment). Data shown as mean  $\pm$ SEM. For all panels \* $P < 0.05$ ; \*\* $P < 0.01$ ; \*\*\* $P < 0.001$ ; \*\*\*\* $P < 0.0001$ .

**Figure 7. Patients display elevated immunosuppressive macrophage signatures in TNBC lung and liver metastatic sites.** (A) Schematic illustration of AURORA US clinical samples from TNBC primary, lung and liver metastatic sites. ( $n = 18$  primary,  $n = 4$  lung and  $n = 4$  liver). (B) Representative heatmap of various immunological and claudin-low/p53 signatures between primary and metastatic tumors from TNBC patients ( $n = 18$  primary,  $n = 4$  lung and  $n = 4$  liver). (C) Gene expression levels of macrophage, neutrophil and EMT signatures between TNBC primary and metastatic tumors ( $n = 18$  primary versus  $n = 8$  metastatic tumors). (D) Volcano plot depicting the most up- and downregulated genes in metastatic samples compared to primary tumors. For all multiple comparisons, p-values were adjusted using the Benjamini-Hochberg method. Gene set analyses were performed using the fgsea package. Gene sets with adjusted p-values  $< 0.05$  were considered significant.

**Figure 8. Novel triple combination promotes adaptive immunity in pre-clinical GEMMs and will now move to a phase 1b clinical trial.** (A) Ablating TAMs with SNDX-ms6352 and immunostimulatory CTX upregulated anti-tumor cytokines (IL-5, IFN- $\gamma$ , CXCL9 and IL-4) while suppressing TAM signatures (*CSF1R*, *TREM2* and *MRC1*) to prolong survival and obtain a CR in primary GEMMs. (B) The addition of anti-PD-1 is required to overcome ITH associated recurrence in double combination treated GEMMs harboring lung metastases. Triple combination treated GEMMs displayed TLSs in the lung while liver metastases had elevated CD8 $^{+}$ , CD4 $^{+}$  T cells and CD20 $^{+}$  B cells with neutrophils surrounding residual tumor cells. (C) The combination of CTX with Axatilimab-csfr (SNDX-ms6352) and Retifanlimab (anti-PD-1) will now be tested as a phase 1b clinical study in TNBC patients with lung and liver metastases.

## REFERENCES

1. Cheang MC, Martin M, Nielsen TO, Prat A, Voduc D, Rodriguez-Lescure A, et al. Defining breast cancer intrinsic subtypes by quantitative receptor expression. *Oncologist*. 2015;20(5):474-82.
2. Schmid P, Adams S, Rugo HS, Schneeweiss A, Barrios CH, Iwata H, et al. Atezolizumab and Nab-Paclitaxel in Advanced Triple-Negative Breast Cancer. *N Engl J Med*. 2018;379(22):2108-21.
3. Emens LA, Adams S, Barrios CH, Diéras V, Iwata H, Loi S, et al. First-line atezolizumab plus nab-paclitaxel for unresectable, locally advanced, or metastatic triple-negative breast cancer: IMpassion130 final overall survival analysis. *Ann Oncol*. 2021;32(8):983-93.
4. Adams S, Loi S, Toppmeyer D, Cescon DW, De Laurentiis M, Nanda R, et al. Pembrolizumab monotherapy for previously untreated, PD-L1-positive, metastatic triple-negative breast cancer: cohort B of the phase II KEYNOTE-086 study. *Ann Oncol*. 2019;30(3):405-11.
5. Hoadley KA, Siegel MB, Kanchi KL, Miller CA, Ding L, Zhao W, et al. Tumor Evolution in Two Patients with Basal-like Breast Cancer: A Retrospective Genomics Study of Multiple Metastases. *PLoS Med*. 2016;13(12):e1002174.
6. Kim IS, Gao Y, Welte T, Wang H, Liu J, Janghorban M, et al. Immuno-subtyping of breast cancer reveals distinct myeloid cell profiles and immunotherapy resistance mechanisms. *Nat Cell Biol*. 2019;21(9):1113-26.
7. Yam C, Abuhadra N, Sun R, Adrada BE, Ding QQ, White JB, et al. Molecular Characterization and Prospective Evaluation of Pathologic Response and Outcomes with Neoadjuvant Therapy in Metaplastic Triple-Negative Breast Cancer. *Clin Cancer Res*. 2022;28(13):2878-89.
8. Yam C, Yen EY, Chang JT, Bassett RL, Alatrash G, Garber H, et al. Immune Phenotype and Response to Neoadjuvant Therapy in Triple-Negative Breast Cancer. *Clin Cancer Res*. 2021.
9. Pagani O, Senkus E, Wood W, Colleoni M, Cufer T, Kyriakides S, et al. International guidelines for management of metastatic breast cancer: can metastatic breast cancer be cured? *J Natl Cancer Inst*. 2010;102(7):456-63.
10. Aftimos P, Oliveira M, Irrthum A, Fumagalli D, Sotiriou C, Gal-Yam EN, et al. Genomic and Transcriptomic Analyses of Breast Cancer Primaries and Matched Metastases in AURORA, the Breast International Group (BIG) Molecular Screening Initiative. *Cancer Discov*. 2021;11(11):2796-811.
11. Garcia-Recio S, Hinoue T, Wheeler GL, Kelly BJ, Garrido-Castro AC, Pascual T, et al. Multiomics in primary and metastatic breast tumors from the AURORA US network finds microenvironment and epigenetic drivers of metastasis. *Nat Cancer*. 2023;4(1):128-47.
12. Guerriero JL, Sotayo A, Ponichtera HE, Castrillon JA, Pourzia AL, Schad S, et al. Class IIa HDAC inhibition reduces breast tumours and metastases through anti-tumour macrophages. *Nature*. 2017;543(7645):428-32.
13. Sun L, Kees T, Almeida AS, Liu B, He XY, Ng D, et al. Activating a collaborative innate-adaptive immune response to control metastasis. *Cancer Cell*. 2021;39(10):1361-74.e9.

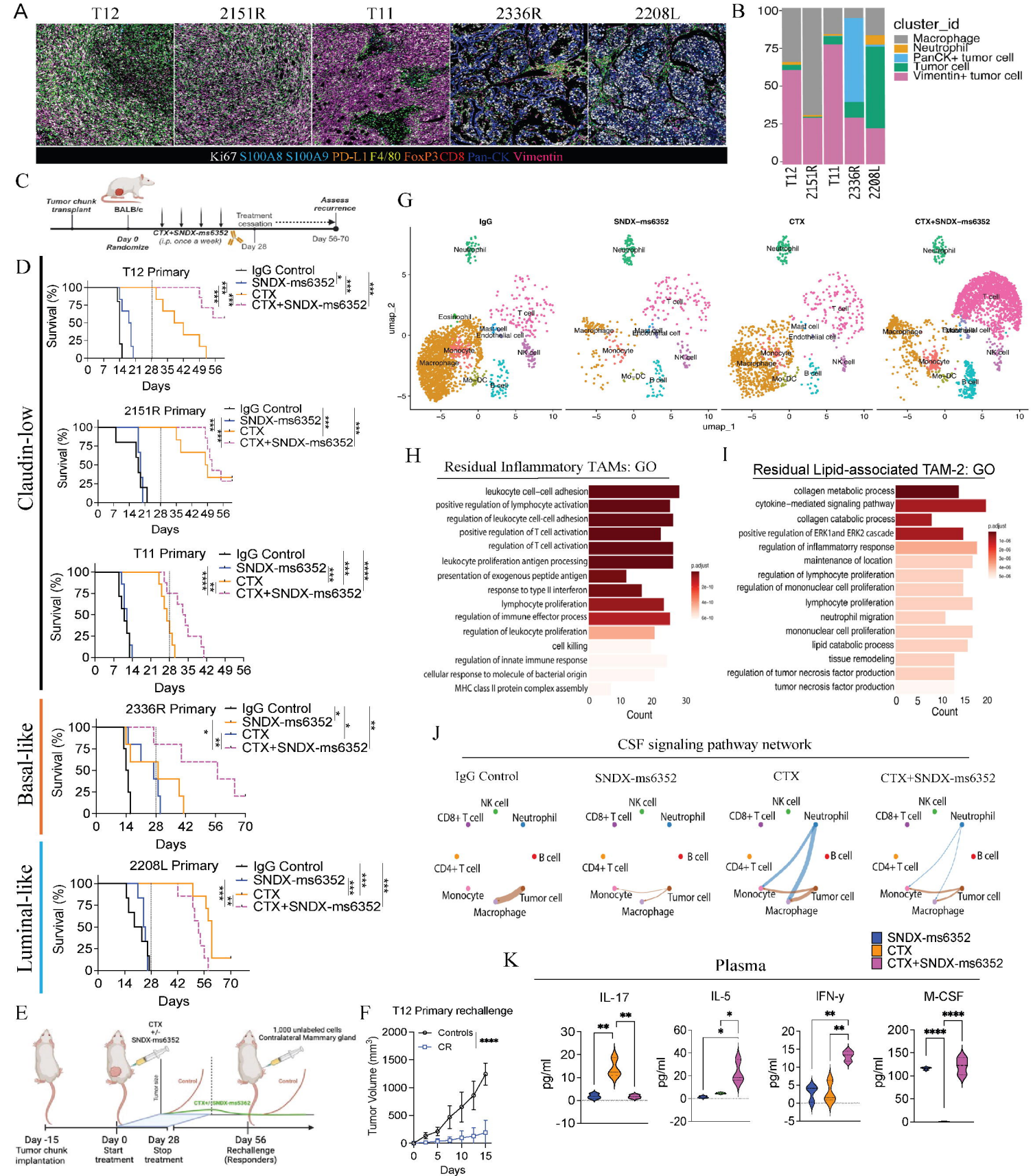
14. Willingham SB, Volkmer JP, Gentles AJ, Sahoo D, Dalerba P, Mitra SS, et al. The CD47-signal regulatory protein alpha (SIRPa) interaction is a therapeutic target for human solid tumors. *Proc Natl Acad Sci U S A.* 2012;109(17):6662-7.
15. Singh S, Lee N, Pedroza DA, Bado IL, Hamor C, Zhang L, et al. Chemotherapy Coupled to Macrophage Inhibition Induces T-cell and B-cell Infiltration and Durable Regression in Triple-Negative Breast Cancer. *Cancer Res.* 2022;82(12):2281-97.
16. Wesolowski R, Sharma N, Reebel L, Rodal MB, Peck A, West BL, et al. Phase Ib study of the combination of pexidartinib (PLX3397), a CSF-1R inhibitor, and paclitaxel in patients with advanced solid tumors. *Ther Adv Med Oncol.* 2019;11:1758835919854238.
17. Ries CH, Cannarile MA, Hoves S, Benz J, Wartha K, Runza V, et al. Targeting tumor-associated macrophages with anti-CSF-1R antibody reveals a strategy for cancer therapy. *Cancer Cell.* 2014;25(6):846-59.
18. Tu MM, Abdel-Hafiz HA, Jones RT, Jean A, Hoff KJ, Duey JE, et al. Inhibition of the CCL2 receptor, CCR2, enhances tumor response to immune checkpoint therapy. *Commun Biol.* 2020;3(1):720.
19. Wang H, Yee D. I-SPY 2: a Neoadjuvant Adaptive Clinical Trial Designed to Improve Outcomes in High-Risk Breast Cancer. *Curr Breast Cancer Rep.* 2019;11(4):303-10.
20. Cassetta L, Fragkogianni S, Sims AH, Swierczak A, Forrester LM, Zhang H, et al. Human Tumor-Associated Macrophage and Monocyte Transcriptional Landscapes Reveal Cancer-Specific Reprogramming, Biomarkers, and Therapeutic Targets. *Cancer Cell.* 2019;35(4):588-602.e10.
21. Beck AH, Espinosa I, Edris B, Li R, Montgomery K, Zhu S, et al. The macrophage colony-stimulating factor 1 response signature in breast carcinoma. *Clin Cancer Res.* 2009;15(3):778-87.
22. Wolff D, Cutler C, Lee SJ, Pusic I, Bittencourt H, White J, et al. Axatilimab in Recurrent or Refractory Chronic Graft-versus-Host Disease. *N Engl J Med.* 2024;391(11):1002-14.
23. Herschkowitz JI, Zhao W, Zhang M, Usary J, Murrow G, Edwards D, et al. Comparative oncogenomics identifies breast tumors enriched in functional tumor-initiating cells. *Proc Natl Acad Sci U S A.* 2012;109(8):2778-83.
24. Olivier M, Langerød A, Carrieri P, Bergh J, Klaar S, Eyfjord J, et al. The clinical value of somatic TP53 gene mutations in 1,794 patients with breast cancer. *Clin Cancer Res.* 2006;12(4):1157-67.
25. Ellis MJ, Ding L, Shen D, Luo J, Suman VJ, Wallis JW, et al. Whole-genome analysis informs breast cancer response to aromatase inhibition. *Nature.* 2012;486(7403):353-60.
26. Razavi P, Chang MT, Xu G, Bandlamudi C, Ross DS, Vasan N, et al. The Genomic Landscape of Endocrine-Resistant Advanced Breast Cancers. *Cancer Cell.* 2018;34(3):427-38.e6.
27. Ma S, Caligiuri MA, Yu J. Harnessing IL-15 signaling to potentiate NK cell-mediated cancer immunotherapy. *Trends Immunol.* 2022;43(10):833-47.
28. Huntington ND, Legrand N, Alves NL, Jaron B, Weijer K, Plet A, et al. IL-15 trans-presentation promotes human NK cell development and differentiation in vivo. *J Exp Med.* 2009;206(1):25-34.

29. Zhang X, Sun S, Hwang I, Tough DF, Sprent J. Potent and selective stimulation of memory-phenotype CD8+ T cells in vivo by IL-15. *Immunity*. 1998;8(5):591-9.
30. Martínez-Sabadell A, Arenas EJ, Arribas J. IFN $\gamma$  Signaling in Natural and Therapy-Induced Antitumor Responses. *Clin Cancer Res*. 2022;28(7):1243-9.
31. Szabo SJ, Sullivan BM, Stemmann C, Satoskar AR, Sleckman BP, Glimcher LH. Distinct effects of T-bet in TH1 lineage commitment and IFN-gamma production in CD4 and CD8 T cells. *Science*. 2002;295(5553):338-42.
32. House IG, Savas P, Lai J, Chen AXY, Oliver AJ, Teo ZL, et al. Macrophage-Derived CXCL9 and CXCL10 Are Required for Antitumor Immune Responses Following Immune Checkpoint Blockade. *Clin Cancer Res*. 2020;26(2):487-504.
33. Bill R, Wirapati P, Messemaier M, Roh W, Zitti B, Duval F, et al. macrophage polarity identifies a network of cellular programs that control human cancers. *Science*. 2023;381(6657):515-24.
34. Nagai S, Toi M. Interleukin-4 and breast cancer. *Breast Cancer*. 2000;7(3):181-6.
35. Zhao J, Chen X, Herjan T, Li X. The role of interleukin-17 in tumor development and progression. *J Exp Med*. 2020;217(1).
36. Murugaiyan G, Saha B. Protumor vs antitumor functions of IL-17. *J Immunol*. 2009;183(7):4169-75.
37. Güç E, Pollard JW. Redefining macrophage and neutrophil biology in the metastatic cascade. *Immunity*. 2021;54(5):885-902.
38. Swierczak A, Cook AD, Lenzo JC, Restall CM, Doherty JP, Anderson RL, et al. The promotion of breast cancer metastasis caused by inhibition of CSF-1R/CSF-1 signaling is blocked by targeting the G-CSF receptor. *Cancer Immunol Res*. 2014;2(8):765-76.
39. Huang R, Wang S, Wang N, Zheng Y, Zhou J, Yang B, et al. CCL5 derived from tumor-associated macrophages promotes prostate cancer stem cells and metastasis via activating  $\beta$ -catenin/STAT3 signaling. *Cell Death Dis*. 2020;11(4):234.
40. Jin L, Han B, Siegel E, Cui Y, Giuliano A, Cui X. Breast cancer lung metastasis: Molecular biology and therapeutic implications. *Cancer Biol Ther*. 2018;19(10):858-68.
41. Vishnoi M, Liu NH, Yin W, Boral D, Scamardo A, Hong D, et al. The identification of a TNBC liver metastasis gene signature by sequential CTC-xenograft modeling. *Mol Oncol*. 2019;13(9):1913-26.
42. Steinbauer M, Guba M, Cernaianu G, Köhl G, Cetto M, Kunz-Schughart LA, et al. GFP-transfected tumor cells are useful in examining early metastasis in vivo, but immune reaction precludes long-term tumor development studies in immunocompetent mice. *Clin Exp Metastasis*. 2003;20(2):135-41.
43. Stripecke R, Carmen Villacres M, Skelton D, Satake N, Halene S, Kohn D. Immune response to green fluorescent protein: implications for gene therapy. *Gene Ther*. 1999;6(7):1305-12.
44. Grzelak CA, Goddard ET, Lederer EE, Rajaram K, Dai J, Shor RE, et al. Elimination of fluorescent protein immunogenicity permits modeling of metastasis in immune-competent settings. *Cancer Cell*. 2022;40(1):1-2.
45. Pedroza DA, Gao Y, Zhang XH, Rosen JM. Leveraging preclinical models of metastatic breast cancer. *Biochim Biophys Acta Rev Cancer*. 2024;1879(5):189163.
46. Black M, Barsoum IB, Truesdell P, Cotechini T, Macdonald-Goodfellow SK, Petroff M, et al. Activation of the PD-1/PD-L1 immune checkpoint confers tumor cell

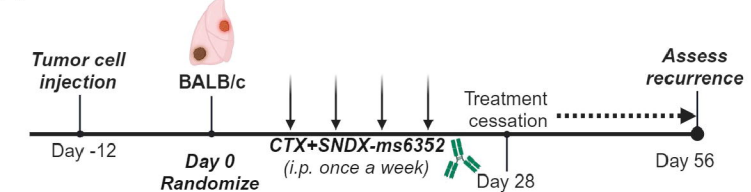
- chemoresistance associated with increased metastasis. *Oncotarget*. 2016;7(9):10557-67.
47. Núñez Abad M, Calabuig-Fariñas S, Lobo de Mena M, Torres-Martínez S, García González C, García García J, et al. Programmed Death-Ligand 1 (PD-L1) as Immunotherapy Biomarker in Breast Cancer. *Cancers (Basel)*. 2022;14(2).
48. Hong M, Kim JW, Kim MK, Chung BW, Ahn SK. Programmed cell death-ligand 1 expression in stromal immune cells is a marker of breast cancer outcome. *J Cancer*. 2020;11(24):7246-52.
49. Zhang M, Sun H, Zhao S, Wang Y, Pu H, Zhang Q. Expression of PD-L1 and prognosis in breast cancer: a meta-analysis. *Oncotarget*. 2017;8(19):31347-54.
50. Cha JH, Chan LC, Li CW, Hsu JL, Hung MC. Mechanisms Controlling PD-L1 Expression in Cancer. *Mol Cell*. 2019;76(3):359-70.
51. Yuan X, Hao X, Chan HL, Zhao N, Pedroza DA, Liu F, et al. CREB-binding protein/P300 bromodomain inhibition reduces neutrophil accumulation and activates antitumor immunity in triple-negative breast cancer. *JCI Insight*. 2024;9(20).
52. Iwase T, Cohen EN, Gao H, Alexander A, Kai M, Chiv V, et al. Maintenance Pembrolizumab Therapy in Patients with Metastatic HER2-negative Breast Cancer with Prior Response to Chemotherapy. *Clin Cancer Res*. 2024;30(11):2424-32.
53. Zhang L, Qiao Z, Yao Y, Li Z, Hu L, Mao Y, et al. A prognostic model for triple-negative breast cancer patients with liver metastasis: A population-based study. *Heliyon*. 2024;10(7):e27837.
54. Xie J, Xu Z. A Population-Based Study on Liver Metastases in Women with Newly Diagnosed Breast Cancer. *Cancer Epidemiol Biomarkers Prev*. 2019;28(2):283-92.
55. Yu J, Green MD, Li S, Sun Y, Journey SN, Choi JE, et al. Liver metastasis restrains immunotherapy efficacy via macrophage-mediated T cell elimination. *Nat Med*. 2021;27(1):152-64.
56. Goddard ET, Fischer J, Schedin P. A Portal Vein Injection Model to Study Liver Metastasis of Breast Cancer. *J Vis Exp*. 2016(118).
57. Sevmis M, Yoyen-Ermis D, Aydin C, Bilgic E, Korkusuz P, Uner A, et al. Splenectomy-Induced Leukocytosis Promotes Intratumoral Accumulation of Myeloid-Derived Suppressor Cells, Angiogenesis and Metastasis. *Immunol Invest*. 2017;46(7):663-76.
58. Crittenden MR, Savage T, Cottam B, Bahjat KS, Redmond WL, Bambina S, et al. The peripheral myeloid expansion driven by murine cancer progression is reversed by radiation therapy of the tumor. *PLoS One*. 2013;8(7):e69527.
59. Cannarile MA, Weisser M, Jacob W, Jegg AM, Ries CH, Rüttinger D. Colony-stimulating factor 1 receptor (CSF1R) inhibitors in cancer therapy. *J Immunother Cancer*. 2017;5(1):53.
60. Xu Y, Zeng H, Jin K, Liu Z, Zhu Y, Xu L, et al. Immunosuppressive tumor-associated macrophages expressing interleukin-10 conferred poor prognosis and therapeutic vulnerability in patients with muscle-invasive bladder cancer. *J Immunother Cancer*. 2022;10(3).
61. Nakamura K, Smyth MJ. TREM2 marks tumor-associated macrophages. *Signal Transduct Target Ther*. 2020;5(1):233.
62. Mathiesen H, Juul-Madsen K, Tramm T, Vorup-Jensen T, Møller HJ, Etzerodt A, et al. Prognostic value of CD163. *Immunol Lett*. 2025;272:106970.

63. Lauwers Y, De Groof TWM, Vincke C, Van Craenenbroeck J, Jumapili NA, Barthelmess RM, et al. Imaging of tumor-associated macrophage dynamics during immunotherapy using a CD163-specific nanobody-based immunotracer. *Proc Natl Acad Sci U S A*. 2024;121(52):e2409668121.
64. Wang H, Shao R, Liu W, Peng S, Bai S, Fu B, et al. Integrative analysis identifies CXCL11 as an immune-related prognostic biomarker correlated with cell proliferation and immune infiltration in multiple myeloma microenvironment. *Cancer Cell Int*. 2022;22(1):187.
65. Torraca V, Cui C, Boland R, Bebelman JP, van der Sar AM, Smit MJ, et al. The CXCR3-CXCL11 signaling axis mediates macrophage recruitment and dissemination of mycobacterial infection. *Dis Model Mech*. 2015;8(3):253-69.
66. Liu M, Fu X, Jiang L, Ma J, Zheng X, Wang S, et al. Colon cancer cells secreted CXCL11 via RBP-Jk to facilitated tumour-associated macrophage-induced cancer metastasis. *J Cell Mol Med*. 2021;25(22):10575-90.
67. Epping MT, Hart AA, Glas AM, Krijgsman O, Bernards R. PRAME expression and clinical outcome of breast cancer. *Br J Cancer*. 2008;99(3):398-403.
68. Chen YL. Prognostic significance of tumor-associated macrophages in patients with nasopharyngeal carcinoma: A meta-analysis. *Medicine (Baltimore)*. 2020;99(39):e21999.
69. Yang Z, Zhang M, Peng R, Liu J, Wang F, Li Y, et al. The prognostic and clinicopathological value of tumor-associated macrophages in patients with colorectal cancer: a systematic review and meta-analysis. *Int J Colorectal Dis*. 2020;35(9):1651-61.
70. Shen H, Liu J, Chen S, Ma X, Ying Y, Li J, et al. Prognostic Value of Tumor-Associated Macrophages in Clear Cell Renal Cell Carcinoma: A Systematic Review and Meta-Analysis. *Front Oncol*. 2021;11:657318.
71. Wang PF, Song SY, Wang TJ, Ji WJ, Li SW, Liu N, et al. Prognostic role of pretreatment circulating MDSCs in patients with solid malignancies: A meta-analysis of 40 studies. *Oncoimmunology*. 2018;7(10):e1494113.
72. Tsujikawa T, Kumar S, Borkar RN, Azimi V, Thibault G, Chang YH, et al. Quantitative Multiplex Immunohistochemistry Reveals Myeloid-Inflamed Tumor-Immune Complexity Associated with Poor Prognosis. *Cell Rep*. 2017;19(1):203-17.
73. DeNardo DG, Brennan DJ, Rexhepaj E, Ruffell B, Shiao SL, Madden SF, et al. Leukocyte complexity predicts breast cancer survival and functionally regulates response to chemotherapy. *Cancer Discov*. 2011;1(1):54-67.
74. Mehta AK, Cheney EM, Hartl CA, Pantelidou C, Oliwa M, Castrillon JA, et al. Targeting immunosuppressive macrophages overcomes PARP inhibitor resistance in BRCA1-associated triple-negative breast cancer. *Nat Cancer*. 2021;2(1):66-82.
75. Generali D, Bates G, Berruti A, Brizzi MP, Campo L, Bonardi S, et al. Immunomodulation of FOXP3+ regulatory T cells by the aromatase inhibitor letrozole in breast cancer patients. *Clin Cancer Res*. 2009;15(3):1046-51.
76. Fares JE, El Tomb P, Khalil LE, Atwani RW, Moukadem HA, Awada A, et al. Metronomic chemotherapy for patients with metastatic breast cancer: Review of effectiveness and potential use during pandemics. *Cancer Treat Rev*. 2020;89:102066.
77. Khan KA, Ponce de Léon JL, Benguigui M, Xu P, Chow A, Cruz-Muñoz W, et al. Immunostimulatory and anti-tumor metronomic cyclophosphamide regimens assessed in primary orthotopic and metastatic murine breast cancer. *NPJ Breast Cancer*. 2020;6:29.

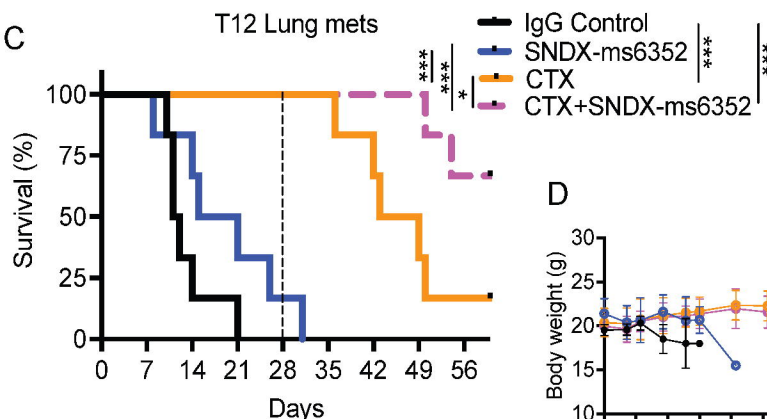
78. Pan Y, Tian T, Park CO, Lofftus SY, Mei S, Liu X, et al. Survival of tissue-resident memory T cells requires exogenous lipid uptake and metabolism. *Nature*. 2017;543(7644):252-6.
79. Lin R, Zhang H, Yuan Y, He Q, Zhou J, Li S, et al. Fatty Acid Oxidation Controls CD8. *Cancer Immunol Res*. 2020;8(4):479-92.
80. Hwang SM, Awasthi D, Jeong J, Sandoval TA, Chae CS, Ramos Y, et al. Transgelin 2 guards T cell lipid metabolism and antitumour function. *Nature*. 2024;635(8040):1010-8.
81. Rosenheim ML. Chronic pyelonephritis. *Isr J Med Sci*. 1967;3(1):93-7.
82. Kesireddy M, Elsayed L, Shostrom VK, Agarwal P, Asif S, Yellala A, et al. Overall Survival and Prognostic Factors in Metastatic Triple-Negative Breast Cancer: A National Cancer Database Analysis. *Cancers (Basel)*. 2024;16(10).
83. Pasha N, Turner NC. Understanding and overcoming tumor heterogeneity in metastatic breast cancer treatment. *Nat Cancer*. 2021;2(7):680-92.
84. Chan LK, Tsui YM, Ho DW, Ng IO. Cellular heterogeneity and plasticity in liver cancer. *Semin Cancer Biol*. 2022;82:134-49.
85. Klughammer J, Abravanel DL, Segerstolpe Å, Blosser TR, Goltsev Y, Cui Y, et al. A multi-modal single-cell and spatial expression map of metastatic breast cancer biopsies across clinicopathological features. *Nat Med*. 2024;30(11):3236-49.
86. Kuett L, Bollhagen A, Tietscher S, Sobottka B, Eling N, Varga Z, et al. Distant Metastases of Breast Cancer Resemble Primary Tumors in Cancer Cell Composition but Differ in Immune Cell Phenotypes. *Cancer Res*. 2025;85(1):15-31.
87. Oberg HH, Wesch D, Kalyan S, Kabelitz D. Regulatory Interactions Between Neutrophils, Tumor Cells and T Cells. *Front Immunol*. 2019;10:1690.
88. Stires H, Bado I, Brown T, Carlson M, Chan IS, Echeverria GV, et al. Improving the odds together: a framework for breast cancer research scientists to include patient advocates in their research. *NPJ Breast Cancer*. 2022;8(1):75.
89. Cortes J, Cescon DW, Rugo HS, Nowecki Z, Im SA, Yusof MM, et al. Pembrolizumab plus chemotherapy versus placebo plus chemotherapy for previously untreated locally recurrent inoperable or metastatic triple-negative breast cancer (KEYNOTE-355): a randomised, placebo-controlled, double-blind, phase 3 clinical trial. *Lancet*. 2020;396(10265):1817-28.
90. Emens LA, Adams S, Cimino-Mathews A, Disis ML, Gatti-Mays ME, Ho AY, et al. Society for Immunotherapy of Cancer (SITC) clinical practice guideline on immunotherapy for the treatment of breast cancer. *J Immunother Cancer*. 2021;9(8).
91. Schmid P, Cortes J, Pusztai L, McArthur H, Kümmel S, Bergh J, et al. Pembrolizumab for Early Triple-Negative Breast Cancer. *N Engl J Med*. 2020;382(9):810-21.
92. Miles D, Gligorov J, André F, Cameron D, Schneeweiss A, Barrios C, et al. Primary results from IMpassion131, a double-blind, placebo-controlled, randomised phase III trial of first-line paclitaxel with or without atezolizumab for unresectable locally advanced/metastatic triple-negative breast cancer. *Ann Oncol*. 2021;32(8):994-1004



A

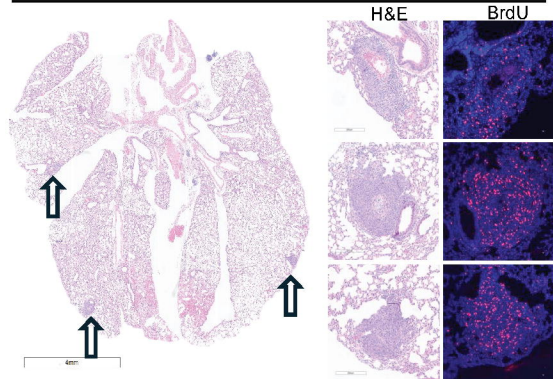


C

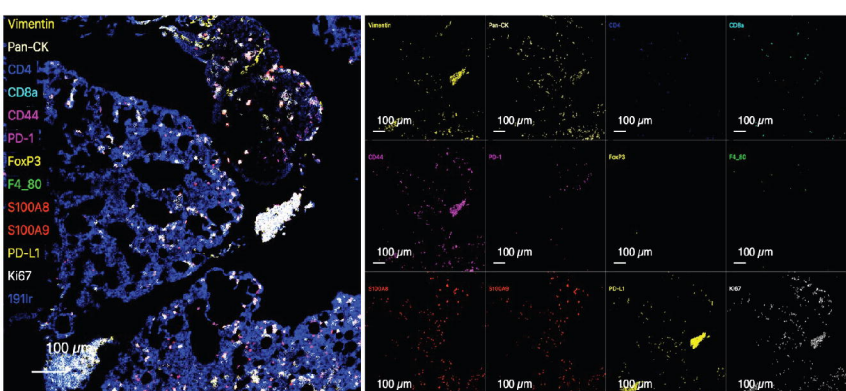
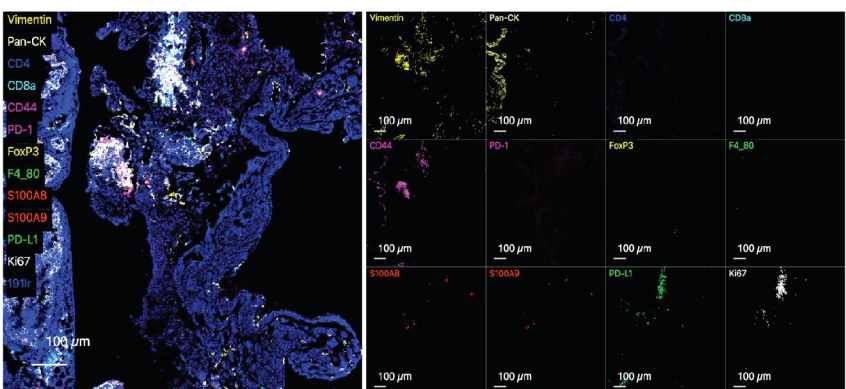


B

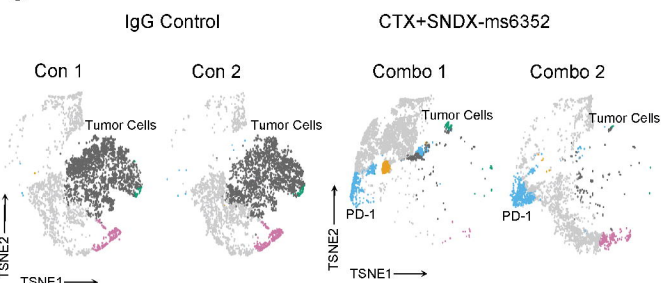
MET ID-Day12



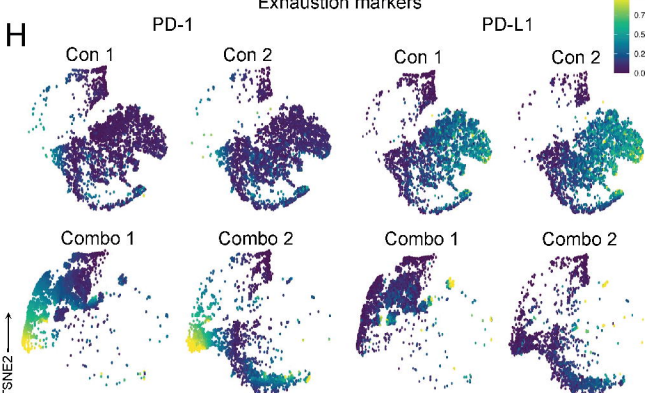
F



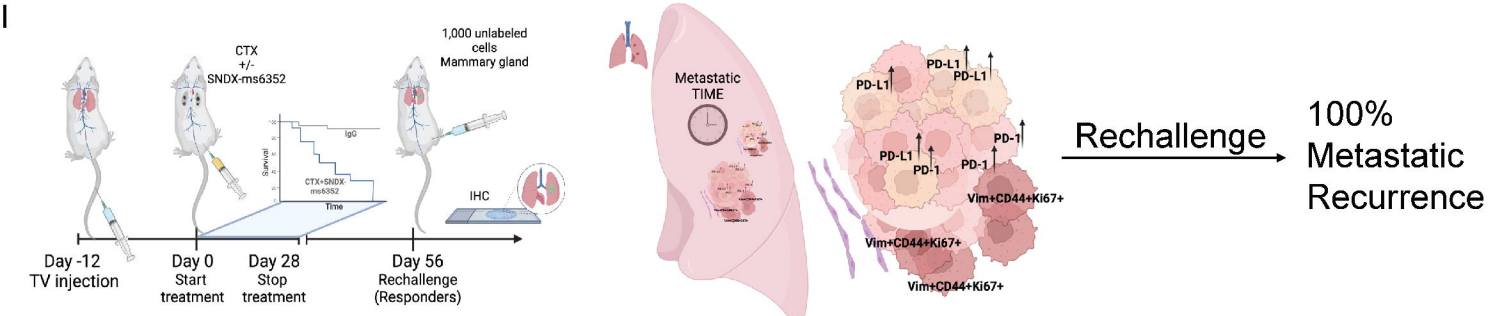
G

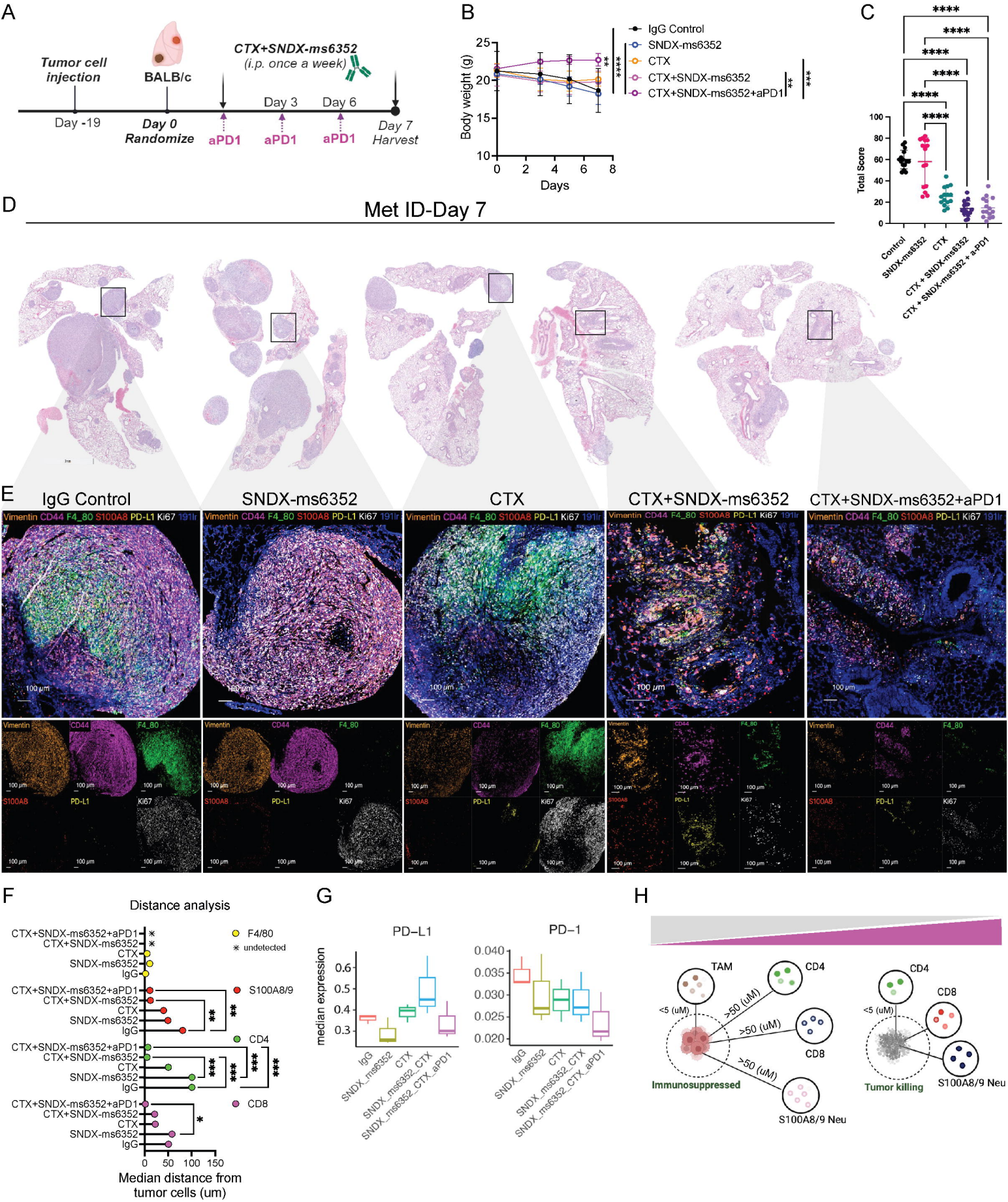


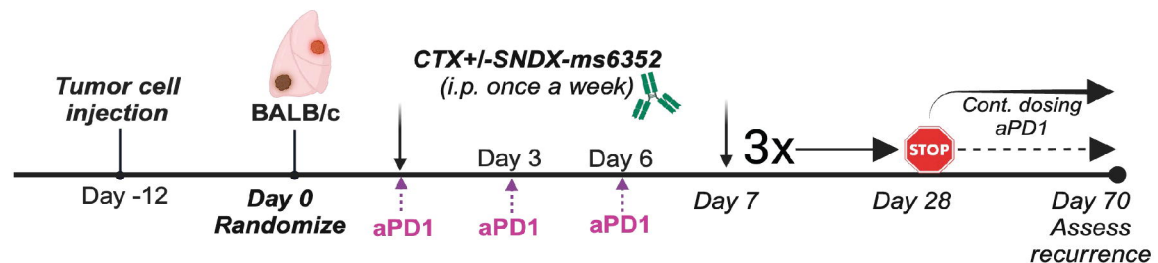
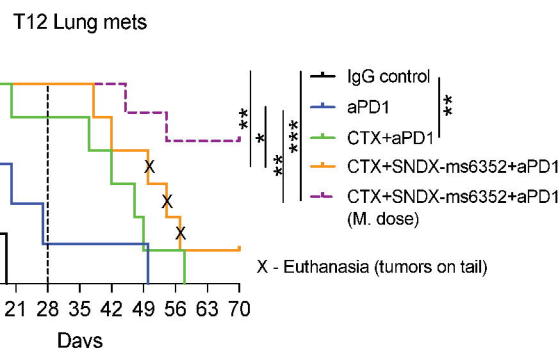
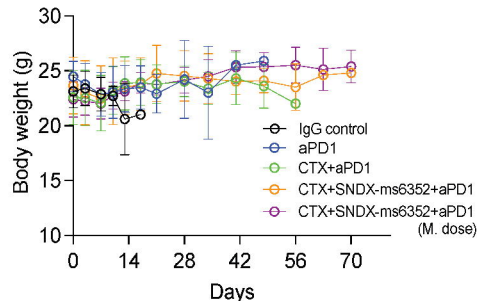
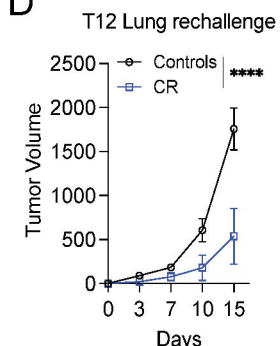
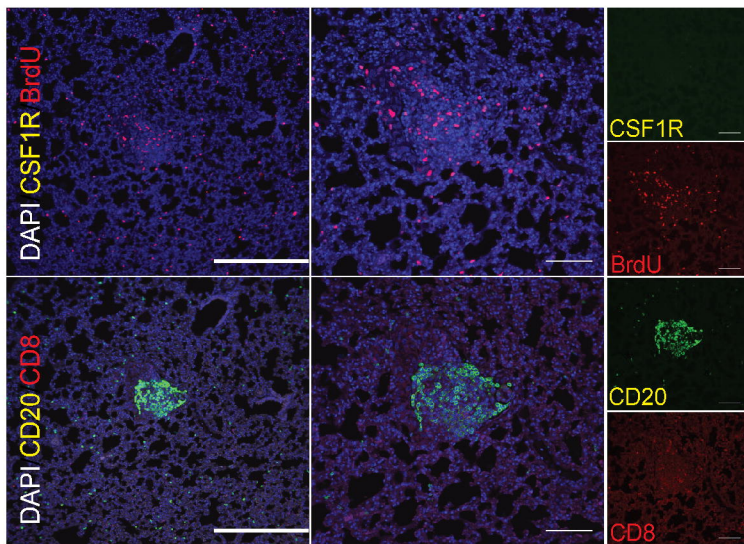
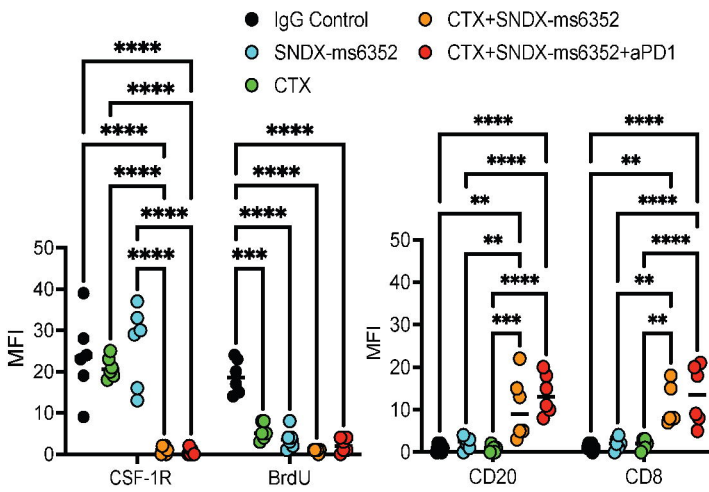
H



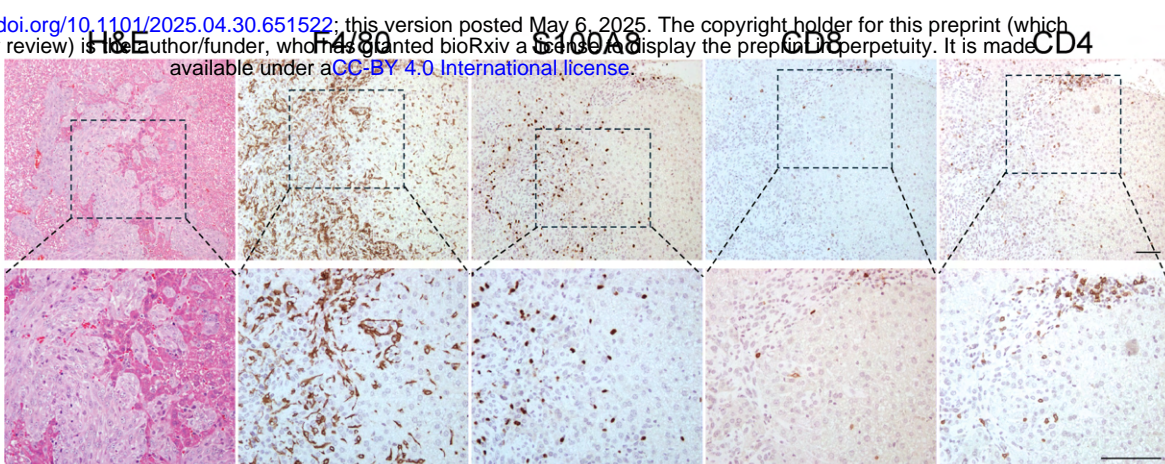
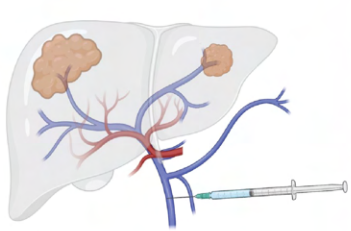
I





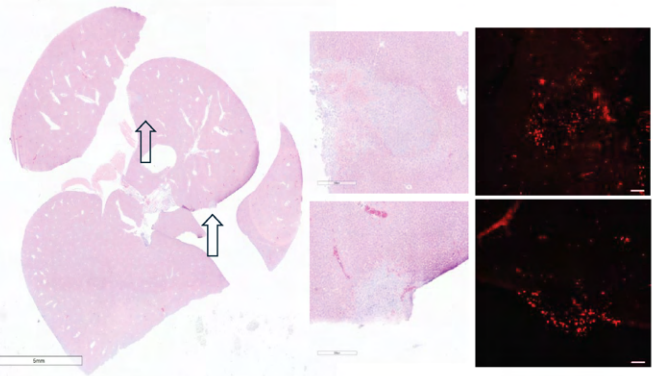
**A****B****C****D****E****F**

A

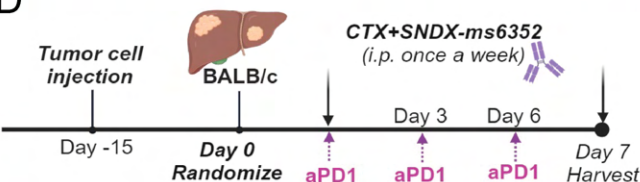


C

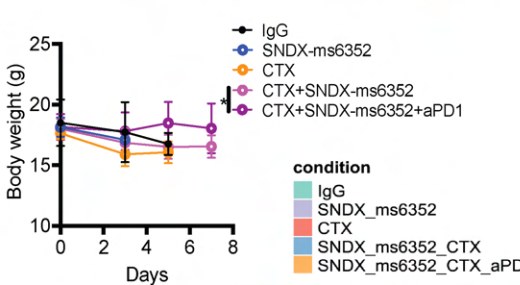
### MET ID-Day 15



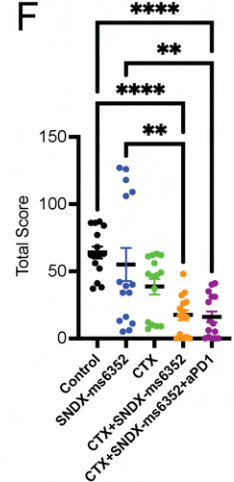
D



E

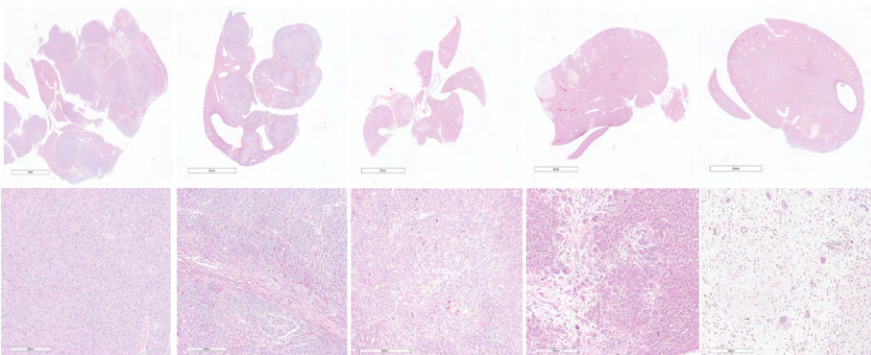


F

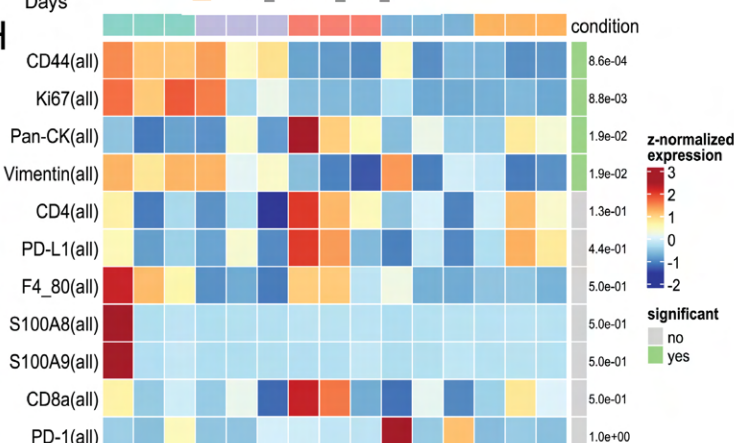


G

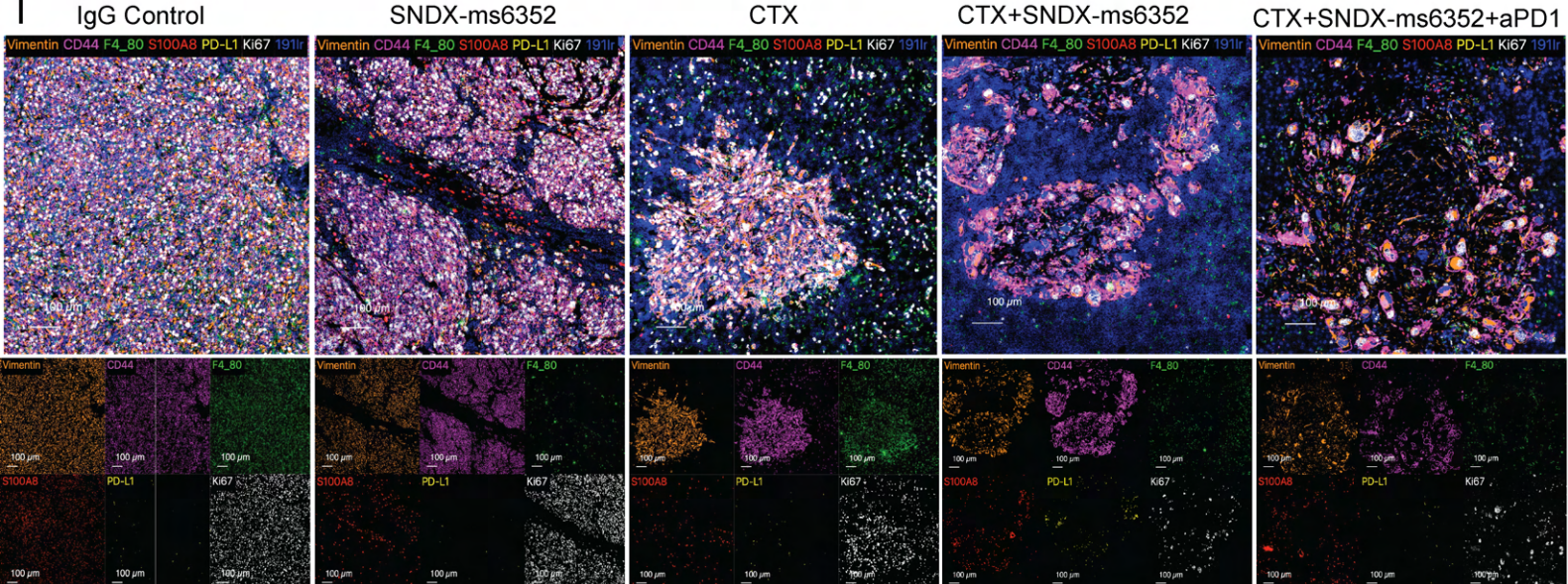
### MET ID-Day 7 (post treatment)

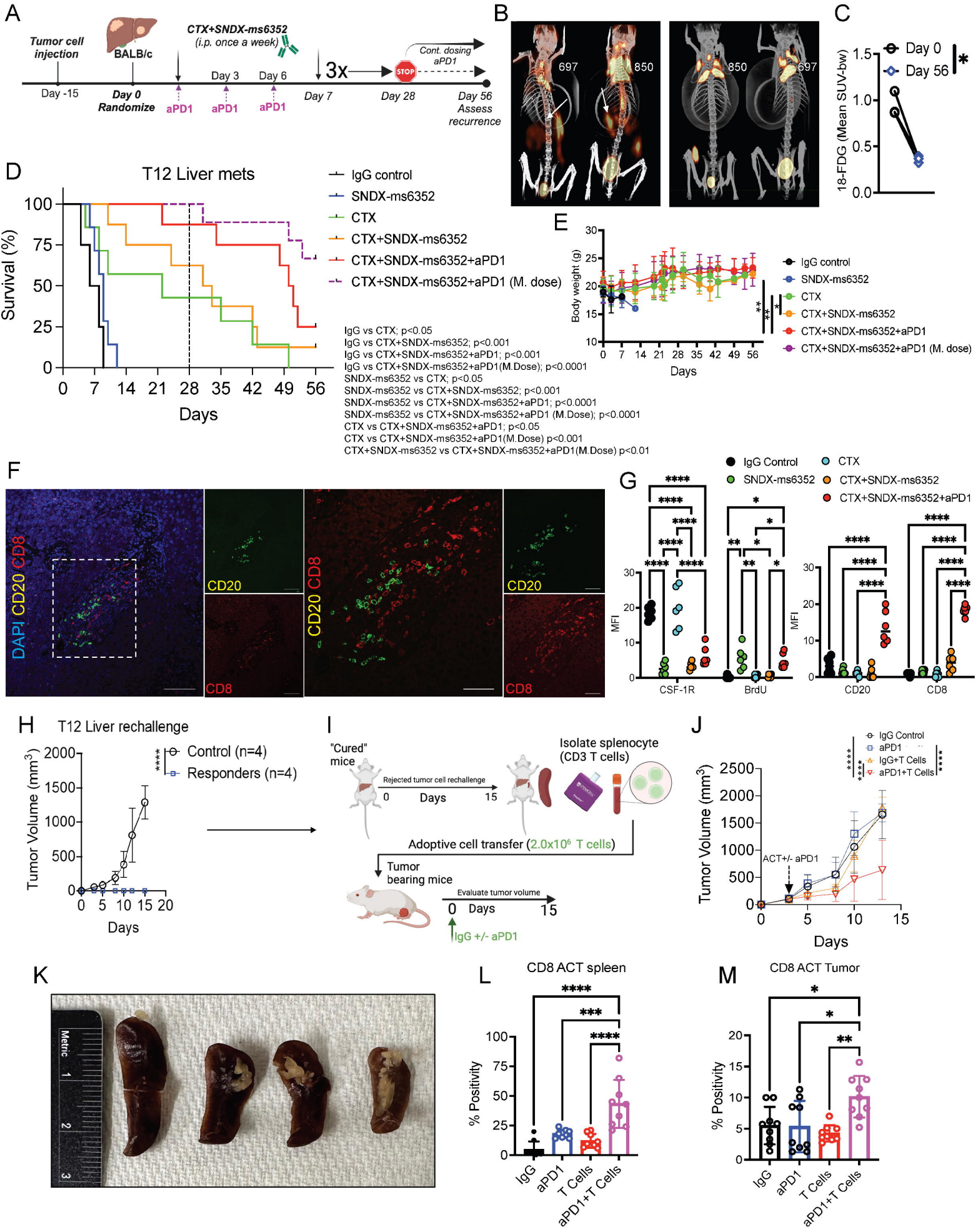


H

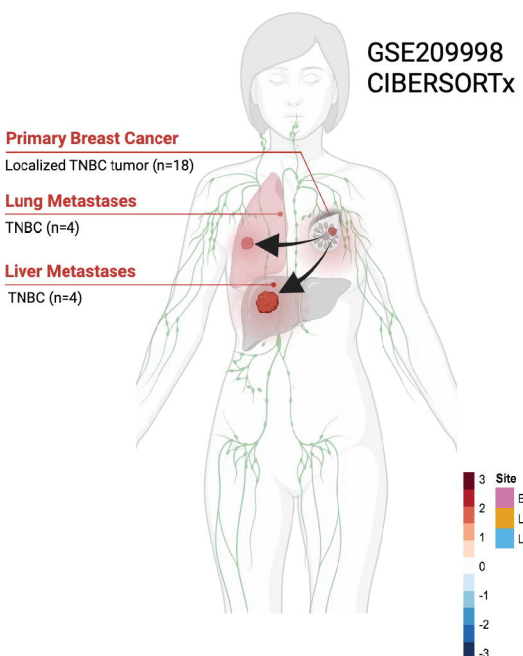


I

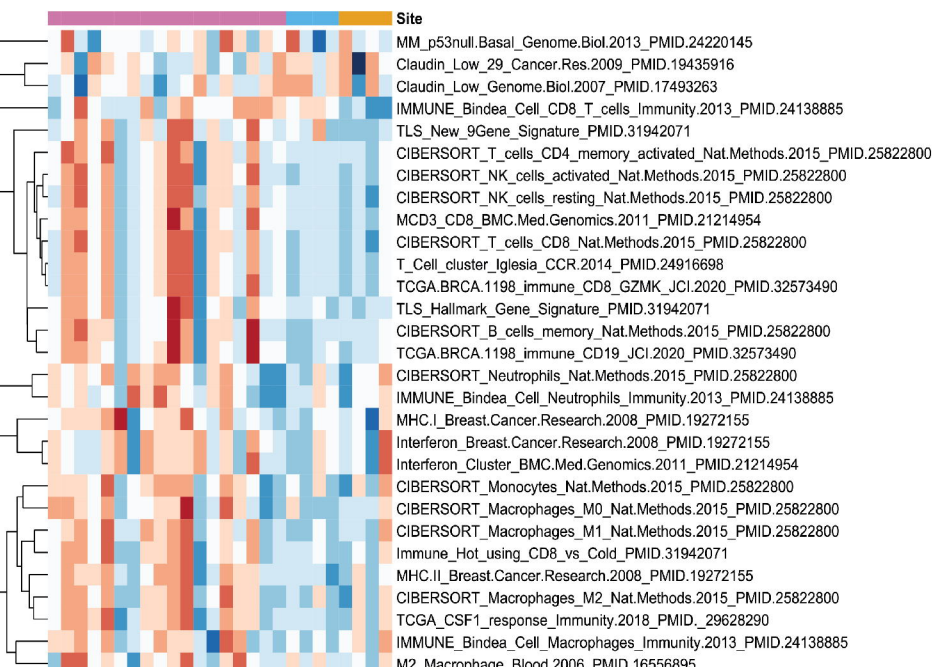




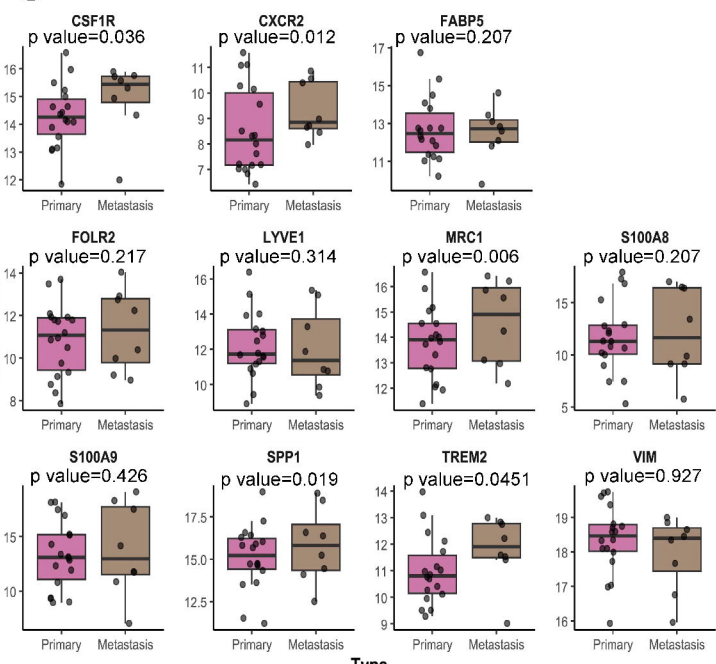
# A AURORA Clinical Samples



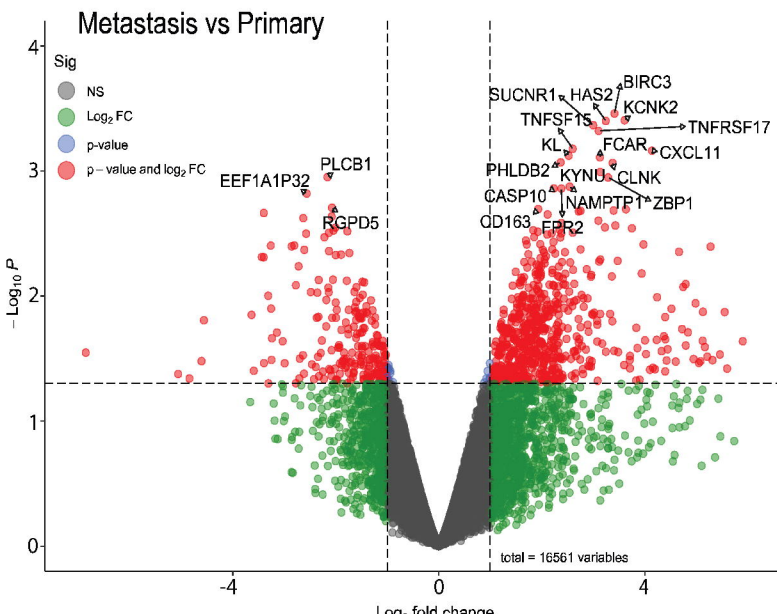
# B TNBC selected modules



# C

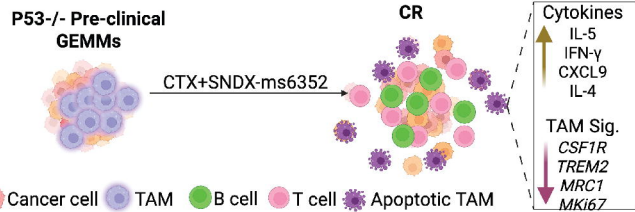


# D



**A**

### Primary Tumors

**B**

### NEW START Phase 1b Clinical Trial

